

# Phase diagram of a graphene bilayer in the zero-energy Landau level

Angelika Knothe<sup>1,2</sup> and Thierry Jolicoeur<sup>1</sup>

1) *Laboratoire de Physique Théorique et Modèles statistiques, Université Paris-Sud, 91405 Orsay, France*

2) *Physikalisches Institut, Albert-Ludwigs-Universität Freiburg,  
Hermann-Herder-Str. 3, D-79104 Freiburg, Germany*

(Dated: September, 2016)

Bilayer graphene under a magnetic field has an octet of quasidegenerate levels due to spin, valley, and orbital degeneracies. This zero-energy Landau level is resolved into several incompressible states whose nature is still elusive. We use a Hartree-Fock treatment of a realistic tight-binding four-band model to understand the quantum ferromagnetism phenomena expected for integer fillings of the octet levels. We include the exchange interaction with filled Landau levels below the octet states. This Lamb-shift-like effect contributes to the orbital splitting of the octet. We give phase diagrams as a function of applied bias and magnetic field. Some of our findings are in agreement with experiments. We discuss the possible appearance of phases with orbital coherence.

## I. INTRODUCTION

The graphene family of new materials has produced novel two-dimensional electron systems. Contrary to semiconductor devices the reduced dimensionality is due to the atomic structure which is made of one or few layers. The bilayer graphene (BLG) has been the subject of intense scrutiny in the last few years. Indeed, it has potential electronic instabilities that are different from those of single-layer graphene<sup>1</sup>. There is a flat band contact at the Fermi level and large Berry curvatures. Several instabilities are competing even for small interactions and it is likely that a layer antiferromagnet is the ground state of the neutral BLG system. This system has very exotic properties under a magnetic field perpendicular to the layers. The Landau levels that appear have a valley degeneracy and in the case of the central zero-energy level there is also an additional degeneracy of two orbital states. When considering also the spin degree of freedom this means that the zero-energy Landau level is eight-fold degenerate, i.e., there is an octet of states at zero energy. Detailed experimental studies<sup>2–11</sup> of the quantum Hall regime of this octet have revealed that the degeneracy is fully lifted presumably by an intricate mixture of one-body effects due to the band structure as well as the Coulomb interactions between electrons. The quantum Hall regime of the octet of states corresponds to Landau level filling factors  $\nu \in [-3, +3]$ . At these fillings there are incompressible states that display various phase transitions when the bias between layers is varied and/or the magnetic field is varied. Some of the gapped states do survive the zero-field limit but this is not always the case. With increasing quality of samples, the fractional quantum Hall effect has also been observed.

For integer fillings of the octet levels we expect the appearance of the well-studied quantum Hall ferromagnetism with the added subtlety of orbital/valley degeneracies<sup>12–14</sup>. From a theoretical point of view, it is sensible to use a Hartree-Fock (HF) approach because in many circumstances the ground state is given by a Slater determinant provided one neglects Landau level mixing. To confront in some detail the experimental results one has to first use a tight-binding model that includes all important couplings including some small particle-hole symmetry breaking terms. When doing a HF calculation it has been pointed out<sup>15</sup> that one has also to include the exchange with the filled Landau levels that form a “Dirac sea” unique to graphene systems. Other theoretical approaches that do not use the quantum Hall ferromagnetism but a gap equation instead have also been applied to the BLG phase diagram<sup>16–18</sup>.

In this paper we use a refined tight-binding model including all dominant hoppings and we treat the exchange effects with the Dirac sea. We derive the phase diagram of the BLG octet as a function of applied bias and magnetic field. Previous recent HF studies either did not take the Dirac sea into account<sup>19</sup> or did not consider all relevant tight-binding hoppings<sup>15</sup>. Here we include the trigonal warping term as well as the next nearest-neighbor interlayer hopping which breaks particle-hole symmetry and also lifts the degeneracy between  $n = 0$  and  $n = 1$  orbitals. We have only searched for spatially uniform phases in the HF solutions. The phase diagrams for all fillings as a function bias and magnetic field are given in Fig. (2). There are many phases whose existence is limited to a very short range of parameters. They are certainly the phases most sensitive to fluctuations beyond HF mean field. So we are more confident about the existence of phases which extend in a large domain. Many of the phases we find can be termed as “incoherent”, i.e., they are Slater determinants of filled levels with eigenstates with well-defined valley ( $\xi$ ), spin ( $\sigma$ ), and orbital quantum numbers ( $n$ ). “Coherent” states involve density matrices with some off-diagonal elements  $\langle c_{X\sigma\xi n}^\dagger c_{X\sigma'\xi'n'} \rangle \neq 0$  for  $\sigma, \xi, n \neq \sigma', \xi', n'$  ( $X$  being the guiding center coordinate).

For filling factors  $\nu = \pm 2$  we find a phase with valley coherence at small bias which is quickly destroyed to give way to incoherent phases. For  $\nu = 0$  an incoherent phase is replaced by a phase with spin and valley coherence for larger bias which then leads to an incoherent state at even larger bias. This is exactly what is found in the simplified

two-band treatment of Lambert and Côté<sup>19</sup>. For odd filling factor, the situation is quite different. For  $\nu = \pm 1$  a phase with valley coherence is replaced by a phase with orbital coherence beyond a critical bias followed then by incoherent phases. For  $\nu = -3$  the situation is similar while for  $\nu = +3$  the small bias regime is now purely an orbital coherent phase and there is no valley coherence. The phases with orbital coherence at  $\nu = \pm 3$  appear for moderate bias and magnetic field, a regime which is plausibly in the range of current experiments.

The paper is organized as follows: in Sec. II, we define the four-band model we employ to describe BLG and describe how we technically proceed to treat the corresponding model Hamiltonian within the HF mean-field picture. In Sec. III, we give the phase diagram for all filling factors of the octet as a function of applied bias and magnetic field. We discuss the phase configurations in terms of spin, valley isospin, and orbital isospin degrees of freedom. In Sec. V the octet polarization properties are discussed for different electronic fillings which leads us to Hund's rules for the successive occupation of the single particle (SP) levels. We further relate these polarization properties to the electronic distribution between the two layers of the system and comment on the possibility of full layer polarization. Finally, we discuss possible extrapolations to stable phases at zero magnetic field. Section VI contains a comparison of our findings to recent experiments as well as to earlier theoretical investigations. In Sec. VII we give some final remarks and present our conclusions.

## II. BACKGROUND AND METHODS

### A. The non-interacting Single Particle Hamiltonian

A sketch of Bernal stacked BLG is shown in Fig. 1. In this model describing BLG as two hexagonal lattices on top of each other, we denote the constituents as follows: It is composed of an upper layer  $L_1$  and a lower layer  $L_2$  separated by interlayer distance  $d$ . In each layer, the hexagonal lattice structure is formed by two trigonal sublattices, in which we label the carbon atoms as  $A$  and  $B$  on the upper layer and  $\tilde{A}$  and  $\tilde{B}$  on the lower layer. This yields a total of four atoms per unit cell. We refer to *dimer* sites if two atoms lie on top of each other and to *non-dimer* sites when this is not the case. A tight binding description of the electrons on this lattice follows from the so-called Slonczewski-Weiss-McClure model of bulk graphite<sup>20,21</sup>. The tight binding hopping parameters are then:  $\gamma_0 = \gamma_{A \leftrightarrow B}$  describes intralayer coupling, *i.e.* next neighbors in-plane hopping within one graphene layer, whereas  $\gamma_1 = \gamma_{\tilde{A} \leftrightarrow B}$  captures interlayer hopping via vertical coupling between the pairs of orbitals on the dimer sites. For the skew interlayer couplings containing both in-plane and vertical components, we write  $\gamma_3 = \gamma_{A \leftrightarrow \tilde{B}}$  for coupling between two non-dimer orbitals and  $\gamma_4 = \gamma_{A \leftrightarrow \tilde{A}}$  for coupling between one dimer and one non-dimer orbital. Due to different on-site energies in BLG, we also include the splitting  $\delta_{A,B}$  for the local energies between  $A$  and  $B$  sites on each layer.

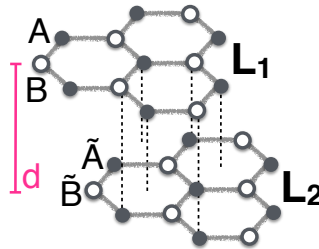


FIG. 1: Sketch of the the model for BLG: Two graphene layers  $L_1$  and  $L_2$  are stacked on top of each other at an interlayer distance  $d$  in the Bernal arrangement. We depict the inequivalent carbon atoms in each monolayer by filled and dashed circles, respectively, and label them as  $A$  ( $\tilde{A}$ ) and  $B$  ( $\tilde{B}$ ) on the upper (lower) layer.

For the hoppings the following relations hold<sup>13,22</sup>:  $\gamma_0 > \gamma_1 > \gamma_3, \gamma_4 \gg \delta_{AB}$ . Throughout this work, we use the numerical values for the parameters listed in Ref. 19 consistent with previous experimental and theoretical investigations<sup>23,24</sup>. In momentum space, we distinguish between the two inequivalent Dirac points  $K$  and  $K'$  and index them by  $\zeta = \pm 1$  following the convention  $\zeta|_K = +1$  and  $\zeta|_{K'} = -1$ . After expanding for small momenta around these Dirac points the effective Hamiltonian describing the low-energy physics can be written as

$$H_\zeta = \zeta \begin{bmatrix} \frac{1}{2}\Delta_B + \frac{1}{2}\zeta(1+\zeta)\delta_{AB} & v_3\mathbf{p} & v_4\mathbf{p}^\dagger & v_0\mathbf{p}^\dagger \\ v_3\mathbf{p}^\dagger & -\frac{1}{2}\Delta_B + \frac{1}{2}\zeta(1+\zeta)\delta_{AB} & v_0\mathbf{p} & v_4\mathbf{p} \\ v_4\mathbf{p} & v_0\mathbf{p}^\dagger & -\frac{1}{2}\Delta_B + \frac{1}{2}\zeta(1-\zeta)\delta_{AB} & \gamma_1 \\ v_0\mathbf{p} & v_4\mathbf{p}^\dagger & \gamma_1 & \frac{1}{2}\Delta_B + \frac{1}{2}\zeta(1-\zeta)\delta_{AB} \end{bmatrix}, \quad (1)$$

acting respectively on the four-component spinor fields

$$\psi_K = \begin{pmatrix} \psi_A \\ \psi_{\tilde{B}} \\ \psi_{\tilde{A}} \\ \psi_B \end{pmatrix} \text{ and } \psi_{K'} = \begin{pmatrix} \psi_{\tilde{B}} \\ \psi_A \\ \psi_B \\ \psi_{\tilde{A}} \end{pmatrix}. \quad (2)$$

In Eq. 1, we use the generalized velocities  $v_i = \frac{\sqrt{3}}{2} \frac{a_L}{\hbar} \gamma_i$  for  $\{i = 0, 1, 3, 4\}$  written in terms of the lattice constant  $a_L$ . Besides,  $\mathbf{p} = p_x + ip_y$ ,  $\mathbf{p}^\dagger = p_x - ip_y$  stands for momentum. Additionally, we want to capture the effect of an externally applied electric field  $E_\perp$ , therefore in Eq. 1 we introduce a bias potential  $\Delta_B = edE_\perp[\frac{mV}{nm}]$ , with  $e$  the electric charge. We now proceed as follows: we first neglect the smaller parameters  $\delta_{AB}, \gamma_3$ , and  $\gamma_4$ . In this case exact analytical solutions can be obtained<sup>15,25-27</sup>. Subsequently, we include the effects of the remaining parameters in first order perturbation theory. The following reasoning closely follows the derivation given in Ref. 15. In the  $K$  valley, the approximate effective Hamiltonian under study reads:

$$H_K = \begin{bmatrix} \frac{1}{2}\Delta_B & 0 & 0 & v_0\mathbf{p}^\dagger \\ 0 & -\frac{1}{2}\Delta_B & v_0\mathbf{p} & 0 \\ 0 & v_0\mathbf{p}^\dagger & -\frac{1}{2}\Delta_B & \gamma_1 \\ v_0\mathbf{p} & 0 & \gamma_1 & \frac{1}{2}\Delta_B \end{bmatrix}. \quad (3)$$

In the presence of a magnetic field of strength  $B$ , we replace the canonical momentum by the mechanical momentum,  $\mathbf{p} \rightarrow \pi = \mathbf{p} + e\mathbf{A}$ , writing the vector potential  $\mathbf{A}$  in Landau gauge,  $\mathbf{A} = Bx\mathbf{e}_y$ . The electronic state quantized into the  $n$ th Landau level is denoted as  $|n\rangle$ , with real space representation at guiding center coordinate  $x_p = p\ell_B^2$  given by

$$\langle \mathbf{r}|n;p\rangle = \frac{1}{\sqrt{L_y}} \phi_n(\mathbf{x} - \mathbf{x}_p) e^{ipy}, \quad (4)$$

where  $\phi_n$  denotes the  $n$ -th harmonic oscillator wave function and  $L_y$  measures the spatial extension of the system in  $y$ -direction. The  $\pi$ -operators act as ladder operators in the space of Landau functions  $\langle \mathbf{r}|n;p\rangle$ ; the corresponding relations

$$\begin{aligned} \pi^\dagger |n\rangle &= i \frac{\hbar}{\ell_B} \sqrt{2(n+1)} |n+1\rangle, \\ \pi |n\rangle &= -i \frac{\hbar}{\ell_B} \sqrt{2n} |n-1\rangle \text{ for } n > 0 \text{ and } \pi|0\rangle = 0, \end{aligned} \quad (5)$$

so the electronic state of the  $n$ -th Landau Level in the valley  $K$  is of the form (agreeing on  $|n\rangle \equiv 0$  for  $n < 0$ )

$$\psi_K^{(n)} = \begin{pmatrix} b_{(n),1}|n\rangle \\ b_{(n),2}|n-2\rangle \\ b_{(n),3}|n-1\rangle \\ b_{(n),4}|n-1\rangle \end{pmatrix}. \quad (6)$$

It is well-known that the LL spectrum of unbiased BLG shows peculiar behavior with respect to the zero energy level<sup>25,26,28</sup>. Indeed, the  $n = 0$  and the  $n = 1$  orbitals have zero energy. As a consequence, the zero energy state of BLG is eight-fold degenerate in the real spin, the valley isospin, and this  $n = 0, 1$  orbital degree of freedom. This property has triggered a plethora of studies to understand the QH ferromagnetism of the zero energy octet of BLG. In the case of biased BLG, strictly speaking, this eight-fold degeneracy is no longer fully exact but broken by the presence of a nonzero bias potential  $\Delta_B$ . As long as the bias potential is sufficiently small compared to the LL gap it is sensible to focus only on the physics of the octet and neglect LL mixing. We assume all the states of energy below the octet states  $\epsilon_{-n} < \epsilon_{0,1} \approx 0$  to be filled. We describe them as a manifold of inert levels  $n \leq -2$  labeled with negative indices and refer to them as the *Dirac sea*. We discuss in more detail the influence of the presence of the Dirac sea electrons in the next section IIB, when interactions between electrons are taken into account. All the states which energetically lie above the pseudo zero energy states with  $\epsilon_n > 0$  are empty. The octet has partial fillings  $\nu \in [-4, 4]$ . For further use we note the explicit forms of the states for the cases  $n = 0$  and  $n = 1$ :

$$\psi_K^{(0)} = \begin{pmatrix} |0\rangle \\ 0 \\ 0 \\ 0 \end{pmatrix}, \quad \psi_K^{(1)} = \begin{pmatrix} b_{(1),1}|1\rangle \\ 0 \\ b_{(1),3}|0\rangle \\ b_{(1),4}|0\rangle \end{pmatrix}, \quad (7)$$

with coefficients

$$\begin{aligned}
b_{(1),1} &= c_1, \\
b_{(1),3} &= -\frac{c_1}{\gamma}(1 - M^2 z^2), \\
b_{(1),4} &= -c_1 z M,
\end{aligned} \tag{8}$$

in terms of the rescaled parameters  $\gamma = \frac{\gamma_1}{\hbar\omega_c}$  and  $2M = \frac{\Delta_B}{\hbar\omega_c}$  and with normalization constant  $c_1 = \frac{1}{\sqrt{1 + \frac{1}{\gamma^2}(1 - M^2 z^2)^2 + z^2 M^2}}$ . Here  $\hbar\omega_c \approx 36.3 v_0 [10^6 \text{ m/s}] \sqrt{B[\text{T}]} \text{ meV}$  is the characteristic cyclotron energy. The parameter  $z$  is determined as the solution in the range  $0 \leq z \leq 1$  to the equation  $z = \frac{1}{\gamma^2}(2 - z)(1 - M^2 z^2)$ . In these expressions, passing from the  $K$  to the  $K'$  valley is done by the replacement  $M \rightarrow -M$ . For the corresponding lowest energy eigenvalues for the  $n = 0$  and the  $n = 1$  orbitals we find

$$\begin{aligned}
\epsilon_{\xi,n=0} &= \xi \frac{1}{2} \Delta_B, \\
\epsilon_{\xi,n=1} &= \xi \frac{1}{2} \Delta_B - \xi \frac{1}{2} z \Delta_B.
\end{aligned} \tag{9}$$

To these solutions of Eq. 9, we compute the corrections due to the parameters  $\delta_{AB}$ ,  $\gamma_3$  and  $\gamma_4$  as perturbations. This is done using the states of Eq. 7 for  $\Delta_B \equiv 0$ . It turns out that taking into account perturbations up to the first order in  $\delta_{AB}$ ,  $\gamma_3$  and  $\gamma_4$  induces a splitting between the  $n = 0$  and the  $n = 1$  orbitals which reads

$$\Delta_{01}^{\text{pert}} = -\delta_{AB}(1 - c^2) - 2 \frac{\gamma_4}{\gamma_0 \gamma_1} c_1^2 (\hbar\omega_c)^2. \tag{10}$$

In addition there is also the Zeeman effect leading to a gap  $\Delta_Z = g\mu_B B$  with  $g = 2$ . Hence, as the main result of this section II A, we write the effects of Eqs. 9, 10, and the Zeeman splitting  $\Delta_Z$  into an effective Hamiltonian describing the  $n = 0, 1$  orbitals of the non-interacting system by writing:

$$H_0 = \sum_p \sum_{n,\sigma,\xi} \left[ -\frac{\Delta_B}{2} \tau_z + z \frac{\Delta_B}{4} (\tau_z + \lambda_z \tau_z) - \frac{\Delta_{01}^{\text{pert}}}{2} \lambda_z - \frac{\Delta_Z}{2} \sigma_z \right] c_{n,\sigma,\xi}^\dagger(p) c_{n,\sigma,\xi}(p), \tag{11}$$

where we use the notation  $\sigma_\alpha = \mathbb{1}^{\text{mode}} \otimes \sigma_\alpha^{\text{spin}} \otimes \mathbb{1}^{\text{valley}}$ ,  $\tau_\alpha = \mathbb{1}^{\text{mode}} \otimes \mathbb{1}^{\text{spin}} \otimes \sigma_\alpha^{\text{valley}}$ , and  $\lambda_\alpha = \sigma_\alpha^{\text{mode}} \otimes \mathbb{1}^{\text{spin}} \otimes \mathbb{1}^{\text{valley}}$  for the Pauli operators acting in spin, in valley, and in orbital space and  $\lambda_\alpha \tau_\beta = \sigma_\alpha^{\text{mode}} \otimes \mathbb{1}^{\text{spin}} \otimes \sigma_\beta^{\text{valley}}$ .

System Parameters			
$\gamma_0$	3.1 eV	$\gamma_1$	0.39 eV
$\gamma_3$	0.1 eV	$\gamma_4$	0.13 eV
$v_0 = \frac{\sqrt{3}}{2} \frac{a_L \gamma_0}{\hbar}$	$1.1 \times 10^6 \text{ m/s}$	$a_L$	0.246 nm
$\hbar\omega_c = \sqrt{2} \frac{\hbar v_F}{\ell_B}$	$36.3 v_0 [10^6 \frac{\text{m}}{\text{s}}] \sqrt{B[\text{T}]} \text{ meV}$	$d$	0.34 nm
$\ell_B = \sqrt{\frac{\hbar c}{eB}}$	$26 \text{ nm} \frac{1}{\sqrt{B[\text{T}]}}$	$\kappa$	5
$\delta_{A,B}$	0.016 eV		
Characteristic energies			
$\Delta_C = \sqrt{\frac{\pi}{2}} \alpha = \sqrt{\frac{\pi}{2}} \frac{e^2}{\kappa \ell_B}$	$14.1 \sqrt{B[\text{T}]} \text{ meV}$	$\Delta_{01}$	$\frac{1}{8} \Delta_C c_1^2 (4 - 3c_1^2)$
$\Delta_Z = g\mu_B B$	$0.11 B[\text{T}] \text{ meV}$	$\Delta_B$	$edE_\perp [\frac{\text{mV}}{\text{nm}}]$

TABLE I: Numerical values of the system parameters and the energy splittings used throughout the analysis.

## B. The Hartree Fock Hamiltonian

We now deal with the Coulomb interaction between the electrons:

$$H_C = \frac{1}{2} \sum_{n,n'} \sum_{\sigma,\sigma'} \sum_{\xi,\xi'} \iint d\mathbf{r} d\mathbf{r}' \Phi_{n1,\sigma,\xi}^\dagger(\mathbf{r}) \Phi_{n2,\sigma',\xi'}^\dagger(\mathbf{r}') V^C(\mathbf{r} - \mathbf{r}') \Phi_{n3,\sigma',\xi'}(\mathbf{r}') \Phi_{n4,\sigma,\xi}(\mathbf{r}), \tag{12}$$

written in terms of the field operator  $\Phi_{n,\sigma,\xi}(\mathbf{r}) = \sum_p \langle \mathbf{r} | n, \sigma, \xi; p \rangle c_{n,\sigma,\xi}(p)$ . As a first approximation to the electron-electron interaction, the fully symmetric potential is  $V^C = \frac{e^2}{\kappa |\mathbf{r}-\mathbf{r}'|}$  with  $\kappa$  the effective dielectric constant can be chosen. A more realistic approach to the specific geometry of the bilayer system is given by a corrected potential which accounts for the finite distance  $d$  between the upper and the lower graphene layer:  $V_{\xi,\xi'}^C = \frac{e^2}{\kappa |\mathbf{r}-\mathbf{r}' + (1-\delta_{\xi,\xi'})d\mathbf{e}_z|}$ , where  $\xi, \xi'$  is the valley index. Note that within the four-band model of BLG, it is not exact to identify the valley index with the sublayer index. We discuss the validity of this approximation below. To keep calculations as simple as possible, we use the corrected Coulomb potential only when it has notable effects. We treat the electron interactions in self-consistent HF theory. We decouple the interaction operator into a direct Hartree part  $H_{C,D}$  and an exchange Fock part  $H_{C,X}$  in the following way:

$$\begin{aligned} H_C &\longrightarrow H_{C,D} + H_{C,X}, \\ \langle c_{n_1,\sigma,K}^\dagger(p_1) c_{n_2,\sigma',K'}^\dagger(p_2) c_{n_3,\sigma,K}(p_3) c_{n_4,\sigma',K'}(p_4) \rangle \\ &\longrightarrow \langle c_{n_1,\sigma,K}^\dagger(p_1) c_{n_4,\sigma',K'}(p_4) \rangle \langle c_{n_2,\sigma,K}^\dagger(p_2) c_{n_3,\sigma',K'}(p_3) \rangle \\ &\quad - \langle c_{n_1,\sigma,K}^\dagger(p_1) c_{n_3,\sigma',K'}(p_3) \rangle \langle c_{n_2,\sigma,K}^\dagger(p_2) c_{n_4,\sigma',K'}(p_4) \rangle. \end{aligned} \quad (13)$$

The technical details of the HF method employed are given in Sec. II C. First, we treat the interactions of the electrons within the octet sector ( $n=0, 1$ ) before analyzing the coupling with the electrons filling the Dirac sea ( $n \leq -2$ ). Within in 01-octet, we consider interaction between the electrons via the corrected potential  $V_{\xi,\xi'}^C = \frac{e^2}{\kappa |\mathbf{r}-\mathbf{r}' + (1-\delta_{\xi,\xi'})d\mathbf{e}_z|}$ . When working with an effective two-band model for the electronic states of BLG<sup>28</sup>, within the zero-mode sector there is a direct one-to-one correspondence between the valley degree of freedom and the electrons occupation in the the upper or the lower layer, respectively<sup>19</sup>. Within the four-band model applied throughout this work, this correspondence valley  $\leftrightarrow$  layer within the pseudo-zero mode sector is no longer exact. Close investigation of the coefficients of Eq. 8 governing the electronic occupation of the different atomic sites on the bilayer lattice reveals the following. The occupation of the different sublayers which would stay fully unoccupied within the two-band model is governed by the coefficient  $b_{(1),3}$  in  $\psi_K^{(1)}$ . The four-band model and the two-band model do predict different behavior of the layer occupation of BLG. This will be of importance in the subsequent discussion. It is thus crucial to take into account the different behavior of the  $n = 0$  and the  $n = 1$  modes within the two models. We estimate the error due to the correspondence valley  $\leftrightarrow$  layer for each valley index: The coefficient  $b_{(1),3}$  is largest in magnitude for zero bias - in this case, the relation  $b_{(1),3}^2 = \frac{b_{(1),1}^2}{\gamma^2}$  holds. Hence,  $b_{(1),3} \ll b_{(1),1}$  since  $\gamma \gg 1$  for the parameters listed in Table I. We therefore use the form of the corrected Coulomb potential  $V_{\xi,\xi'}^C$  given above in order to include the effect of the anisotropic Coulomb interaction due to the finite separation between the layers. We perform the HF decoupling of the Coulomb-interaction term in the four-band model as calculations within an effective two-band model of BLG presented in 14 and 19. The contribution from the direct interaction term competes with a positive, neutralizing background and yields a capacitive energy<sup>19</sup>

$$H_{D, \text{Octet}} = \sum_p \sum_{n,\sigma,\xi} \alpha \frac{d}{\ell_B} \left( \tilde{v}_\xi - \frac{\tilde{v}}{2} \right) c_{n,\sigma,\xi}^\dagger(p) c_{n,\sigma,\xi}(p), \quad (14)$$

where we denote with  $\tilde{v}_\xi = \sum_p \sum_{n\sigma} \langle c_{n,\sigma,\xi}^\dagger(p) c_{n,\sigma,\xi}(p) \rangle$  the total filling in valley  $\xi$ ,  $\tilde{v} = \nu + 4$  counts the total number of filled levels in the octet, and  $\alpha = \frac{e^2}{\kappa \ell_B}$ . From the exchange part of the interaction we obtain the contribution

$$H_{X, \text{Octet}} = - \sum_{\substack{p_1,p_2 \\ p_3,p_4}} \sum_{\substack{n_1,n_3 \\ n_2,n_4}} \sum_{\substack{\sigma,\xi \\ \sigma',\xi'}} \mathfrak{X}_{n_1,n_3}^{\xi,\xi'}(0) \langle c_{n_1,\sigma,\xi}^\dagger(p_1) c_{n_3,\sigma',\xi'}(p_3) \rangle \langle c_{n_2,\sigma',\xi'}^\dagger(p_2) c_{n_4,\sigma,\xi}(p_4) \rangle, \quad (15)$$

where, following previous definitions, we find the exchange matrix elements

$$\mathfrak{X}_{n_1,n_2}^{\xi,\xi'}(\mathbf{q}) = \alpha \int \frac{d\mathbf{p} \ell_B^2}{2\pi} \frac{1}{p \ell_B} e^{-pd(1-\delta_{\xi,\xi'})} \mathfrak{K}_{n_1,n_4}(p) \mathfrak{K}_{n_3,n_2}(-p) e^{i\mathbf{p} \times \mathbf{q} \ell_B^2}, \quad (16)$$

with

$$\begin{aligned}
\mathfrak{K}_{0,0}(\mathbf{p}) &= e^{-\frac{\ell_B^2 p^2}{4}} \\
\mathfrak{K}_{0,1}(\mathbf{p}) &= e^{-\frac{\ell_B^2 p^2}{4}} \frac{c_1 \ell_B}{\sqrt{2}} (ip_x + p_y) \\
\mathfrak{K}_{1,0}(\mathbf{p}) &= e^{-\frac{\ell_B^2 p^2}{4}} \frac{c_1 \ell_B}{\sqrt{2}} (ip_x - p_y) \\
\mathfrak{K}_{1,1}(\mathbf{p}) &= e^{-\frac{\ell_B^2 p^2}{4}} (1 - c_1 \frac{\ell_B^2 p^2}{2}).
\end{aligned} \tag{17}$$

For future use we introduce the notation  $\Delta_{n_1 n_2 n_3 n_4} := \mathfrak{X}_{n_1, n_2, n_3, n_4}^{\xi, \xi'}$  for the terms conserving the valley index and  $X_{n_1 n_2 n_3 n_4} := \mathfrak{X}_{n_1, n_2, n_3, n_4}^{\xi, \xi'}$  in the case  $\xi \neq \xi'$  for the valley index non-conserving terms.

In Ref. 15, Shizuya has shown that exchange interactions between the electrons in the Dirac sea within the four-band model of BLG leads to a splitting  $\Delta_{01}^{\text{int}}$  between the  $n = 0$  and  $n = 1$  orbitals. This exchange phenomenon analogous to the Lamb shift of atomic energy levels leads to a term of the form (where the LL index only runs over  $n = 0, 1$ ):

$$H_{X, \text{Dirac}} = \sum_p \sum_{n, \sigma, \xi} \frac{\Delta_{01}^{\text{int}}}{2} \lambda_z c_{n, \sigma, \xi}^\dagger(p) c_{n, \sigma, \xi}(p), \tag{18}$$

with  $\lambda_\alpha = \sigma_\alpha^{\text{mode}} \otimes \mathbb{1}^{\text{spin}} \otimes \mathbb{1}^{\text{valley}}$  for the Pauli operators acting in 01-orbital space and  $\Delta_{01}^{\text{int}} = \frac{1}{8} \Delta_C c_1^2 (4 - 3c_1^2)$  is the splitting induced by the presence of the Dirac sea, where we defined  $\Delta_C = \sqrt{\frac{\pi}{2}} \alpha = \sqrt{\frac{\pi}{2}} \frac{e^2}{\kappa \ell_B}$ .

Considering the anisotropic interlayer Coulomb interaction merely entails a simple rescaling (at first order in  $d/\ell_B$ )  $\Delta_B \rightarrow \Delta_{B, \text{eff}} = (1 - 16 \frac{W}{\hbar \omega_c}) \Delta_B$ . Assembling all terms from above discussion, we arrive at the HF Hamiltonian

$$H_{HF} = H_0 + H_{X, \text{Octet}} + H_{D, \text{Octet}} + H_{X, \text{Dirac}}. \tag{19}$$

Hence, in terms of the order parameter  $P_{n', n, \sigma', \xi', \xi}(p) := \langle c_{n, \sigma, \xi}^\dagger(p) c_{n', \sigma', \xi', \xi}(p) \rangle$ , and within a local approximation  $P(p) \approx P(p')$  for a state uniform or varying sufficiently slowly in space, we obtain for the HF energy functional (suppressing summation over  $p$ ):

$$\begin{aligned}
E_{HF} &= -\frac{1}{2} \sum_{\substack{n_1, n_3 \\ n_2, n_4}} \sum_{\substack{\sigma, \xi \\ \sigma', \xi'}} \mathfrak{X}_{n_1, n_3, n_2, n_4}^{\xi, \xi'}(0) P_{n_3, n_1, \sigma', \sigma, \xi', \xi} P_{n_4, n_2, \sigma, \sigma', \xi, \xi'} + \frac{\alpha}{4} \frac{d}{\ell_B} (\tilde{\nu}_K - \tilde{\nu}_{K'})^2 \\
&+ \frac{\Delta_{01}}{2} \text{Tr}[\lambda_z P] + \frac{\Delta_Z}{2} \text{Tr}[\sigma_z P] + \frac{\Delta_{B, \text{eff}}}{2} \text{Tr}[\tau_z P] + z \frac{\Delta_{B, \text{eff}}}{4} \text{Tr}[(\tau_z + \lambda_z \tau_z) P],
\end{aligned} \tag{20}$$

where we summarized  $\Delta_{01} = \Delta_{01}^{\text{pert}} + \Delta_{01}^{\text{int}}$  as the total splitting in orbital space induced by the different effects discussed above. We search only uniform HF solutions.

### C. HF method

In this work, we study the model Hamiltonian  $H_{HF}$  given in Eq. 19 within HF theory. In Eq. 19, the Hamiltonian  $H_{HF}$  depends on  $P$  which in turn itself is determined by the lowest-energy solution to the corresponding eigenvalue problem. The numerical procedure leading to its solution must thus be carried out self-consistently. We briefly sketch the algorithm used in our analysis. We fix the total number of electrons in the octet. Here, the *filling factor*  $\nu$  of the octet is defined with respect to the half-filled, charge neutral case: We write  $\nu = -3$  ( $-2, -1, 0, 1, 2, 3$ ) for 1 ( $2, 3, 4, 5, 6, 7$ ) out of the eight available zero-energy levels being occupied. In Secs. III and V, we present investigations and discussions of all the different possible fillings factors  $\nu \in [-3, 3]$ . The density matrix is assumed to be independent of the guiding center coordinate so we are looking only for spatially uniform solutions. For a given filling factor  $\nu$  implying  $n$  occupied levels, we start by initializing  $n$  SP vectors  $|i\rangle$ : The eight entries each are taken from a random uniform distribution, thereby respecting normalization. The density matrix  $P^{\text{int}} = \sum_i^n |i\rangle \langle i|$  built from these vectors serves as a starting point for the self-consistent HF minimization procedure.

Iteration schemes similar to the one used here and equally based on the so-called Roothaan algorithm for self-consistent HF iteration<sup>29</sup> have been applied earlier in HF studies of QH systems<sup>30,31</sup>.

A check for proper convergence to a true solution of the HF equations is performed by always requiring the SP energy eigenvalues to reproduce the energy yielded by the HF energy functional of Eq. 20 up to a precision better than  $10^{-5}$ .

From the final converged density matrix  $P$  we calculate the components of the spin  $\mathbf{S}$ , the valley isospin  $\mathbf{T}$ , and the orbital isospin degree of freedom  $\mathbf{L}$  according to

$$S_\alpha = \frac{1}{2}\text{Tr}[\sigma_\alpha P], \quad T_\alpha = \frac{1}{2}\text{Tr}[\tau_\alpha P], \quad L_\alpha = \frac{1}{2}\text{Tr}[\lambda_\alpha P], \quad (21)$$

for  $\alpha \in \{x, y, z\}$ . We identify different phases by different configurations of the spin and isospin degrees of freedom. By tracing their evolution as functions of the external parameters, i.e., the bias potential  $\Delta_B$  and the magnetic field  $B$ , we determine the phase diagrams in the  $\{\Delta_B-B\}$ -plane. From this numerical HF procedure we furthermore gain information about the HF SP eigenstates and eigenvalues for each value of  $\Delta_B$  and  $B$ . Hence we can infer the structure of the occupied and unoccupied SP states for each phase within this HF MF picture. This knowledge about the GS structure allows us to proceed further by analytical means: Using a particular structure of the GS eigenvectors to construct the corresponding density matrix  $P$  and minimizing the HF energy functional given in Eq. 20 for this  $P$ , allows us to compute analytically properties of the various phases such as canting angles of the energetically favorable spin and isospin orientation or phase boundaries between different GS phases.

We have not tried to search for spatially non-uniform HF solutions. There is no clear experimental evidence for such states so far. The HF investigations of Lambert and Côté have found such solutions only at very large bias.

### III. HF PHASE DIAGRAM

We present the phase diagrams of BLG obtained for different filling factors  $\nu$  using the HF procedure described in the previous section II C. In Fig. 2, we plot the phase diagrams for the different  $\nu$  in the plane spanned by the bias  $\Delta_B$  and the magnetic field  $B$ . From these phase diagrams, we identify a total of 32 different phases of the BLG system at different filling factors. The explicit form of the respective phases are listed in Tables II-VIII. Their spin and isospin polarization properties are given in Tables IX and X for negative and positive filling factors, respectively. In the first section of the text, we successively discuss the respective cases for each different filling factor. We next summarize these results and compare our findings for different  $\nu$  among each other.

Figure 2 shows the collection of phase diagrams obtained for the different filling factors  $\nu \in [-3, 3]$ .

#### A. One electron: $\nu = -3$

With one electron per orbital in the system, we find the following different phases:

Unbiased case ( $\Delta_B \equiv 0$ , evolution as a function of  $B$ ): the GS is polarized along the  $z$ -axis in the spin degree of freedom, but not in the valley degree of freedom, where the corresponding isospin vector lies in the  $\{x-y\}$ -plane. The isospin corresponding to the orbital mode is in a canted configuration, thus we find a phase with orbital coherence. The optimal canting angle in orbital space  $\theta_0$ , plotted in Fig. 5, varies as a function of  $B$  between  $\theta_0 \rightarrow \frac{\pi}{4}$  at vanishing magnetic field and  $\theta_0 \equiv 0$  at sufficiently high magnetic field strengths above a certain critical value  $B_{crit} \approx 11$  T. It is given by the relation

$$\cos \theta_0 = \frac{\sqrt{-\Delta_{0011} + 2\Delta_{01} - \Delta_{1001} + \Delta_{0000} - X_{0011} - X_{1001} + X_{0000}}}{\sqrt{\Delta_{0000} - 2\Delta_{0011} - 2\Delta_{1001} + \Delta_{1111} + X_{0000} - 2X_{0011} - 2X_{1001} + X_{1111}}}. \quad (22)$$

Along the line of zero bias, the GS hence undergoes a transition from a canted to a fully polarized state in orbital isospin with increasing magnetic field strength  $B$ .

Phase (I) occurs at small but nonzero bias  $\Delta_B > 0$  and below a critical magnetic field strength  $B < B_{crit}$ : the GS is spin polarized and canted both in valley and orbital degrees of freedom. In phase (I), cuts along lines of increasing bias  $\Delta_B$ , for any strength of the magnetic field  $B$ , correspond to a rotation of the valley-isospin vector from a configuration in the  $\{x-y\}$ -plane to a state fully polarized along the  $z$ -axis. At the same time, there is orbital coherence, the orbital isospin components taking non-trivial values  $0 < L_x, L_z < 1$ .

Phase (II): still in the regime of very small values of the bias  $\Delta_B$ , but for larger magnetic fields  $B > B_{crit}$ , the system is fully polarized in the spin and orbital isospin degree of freedom. The valley isospin, however, is in a canted

$\Delta_B \equiv 0$	$ v_1\rangle = \frac{1}{\sqrt{2}} \cos \theta \left[  1, \uparrow, +\rangle +  1, \uparrow, -\rangle \right] + \frac{1}{\sqrt{2}} \sin \theta \left[  0, \uparrow, +\rangle +  0, \uparrow, -\rangle \right]$
Phase (I)	$ v_1\rangle = a_1 1, \uparrow, +\rangle + a_2 1, \uparrow, -\rangle + a_5 0, \uparrow, +\rangle + a_6 0, \uparrow, -\rangle$
Phase (II)	$ v_1\rangle = \sin \theta  1, \uparrow, +\rangle + \cos \theta  1, \uparrow, -\rangle$
Phase (III)	$ v_1\rangle =  1, \uparrow, +\rangle$
Phase (IV)	$ v_1\rangle = \sin \theta  1, \uparrow, +\rangle + \cos \theta  0, \uparrow, +\rangle$
Phase (V)	$ v_1\rangle =  0, \uparrow, +\rangle$

TABLE II: GS configurations for the different phases for filling factor  $\nu = -3$ .

configuration, where the optimal angle is determined by

$$\cos 2\theta_{II} = \frac{\Delta_{B,eff} \ell_B (z - 1)}{\alpha d + \ell_B (\Delta_{1111} - X_{1111})}. \quad (23)$$

Hence, in phase (II), along any cut at a fixed  $B > B_{crit}$ , as the bias  $\Delta_B$  increases, the state undergoes a rotation of the valley-isospin from  $\mathbf{T}$  lying in the  $\{x-y\}$ -plane at  $\Delta_B = 0$  to a fully valley polarized state at sufficiently large  $\Delta_B$ .

Phase (III) emerges as an intermediate phase at sufficiently large values of the magnetic field  $B > B_{crit} \approx 11$  T when the bias potential is raised beyond the regime of phase (II): over a certain parameter range of bias and magnetic field strength, the system becomes a fully polarized ferromagnet in all spins and isospins.

Phase (IV) dominates the intermediate part of the  $\nu = -3$  phase diagram over the whole parameter range of bias  $\Delta_B$  and magnetic field strength  $B$ . It is characterized by full ferromagnetic polarization of the spin and valley isospin, but canting of the orbital isospin resulting in an orbital coherent phase. For the optimal canting angle in orbital space we find the expression

$$\cos 2\theta_{IV} = \frac{-\Delta_{0000} - 2\Delta_{01} + \Delta_{1111} + z\Delta_{B,eff}}{\Delta_{0000} - 2\Delta_{0011} - 2\Delta_{1001} + \Delta_{1111}}. \quad (24)$$

In phase (IV), cuts as a function of increasing bias  $\Delta_B$  at any value of the magnetic field hence trace the rotation of the orbital isospin vector to the fully antiferromagnetically-polarized state in orbital space.

Phase (V): for sufficiently large values of the bias, we find the limiting case for the GS to be fully polarized in spin and valley isospin, but antiferromagnetically-polarized in the orbital degree of freedom. At  $\nu = -3$ , all phases transform into one another via smooth rotations of the respective isospin degrees of freedom. All transitions between different phases therefore are of second order in this case. These phase transitions occur at the following critical values of the bias, respectively:

(II)  $\rightarrow$  (III):

$$\Delta_{B,eff}^{crit} = \frac{-\alpha d - \Delta_{1111}\ell_B + \ell_B X_{1111}}{\ell(z - 1)}, \quad (25)$$

(III)  $\rightarrow$  (IV):

$$\Delta_{B,eff}^{crit} = \frac{2}{z}(\Delta_{0011} + \Delta_{01} + \Delta_{1001} - \Delta_{1111}), \quad (26)$$

(IV)  $\rightarrow$  (V):

$$\Delta_{B,eff}^{crit} = \frac{2}{z}(\Delta_{0000} - \Delta_{0011} + \Delta_{01} - \Delta_{1001}). \quad (27)$$

## B. Two electrons: $\nu = -2$

When there are two electrons per state within the octet, the GS structure of the system is the following:

Phase (I): for small values of the bias  $\Delta_B < \Delta_B^{crit}$ , the GS is partially polarized in the spin, whereas the valley isospin is canted and the orbital isospin is ordered in an antiferromagnetic way. The optimal valley canting angle is determined by

$$\cos 2\theta_I = \frac{\Delta_{B,eff}\ell_B(z - 2)}{-4\alpha d - \Delta_{0000}\ell_B - 2\Delta_{0011}\ell_B - \Delta_{1111}\ell_B + \ell_B X_{0000} + 2\ell_B X_{0011} + \ell_B X_{1111}}. \quad (28)$$



$\Delta_B \equiv 0$	$ v_1\rangle = \frac{1}{\sqrt{2}}[ 1, \uparrow, +\rangle +  1, \uparrow, -\rangle],  v_2\rangle = \frac{1}{\sqrt{2}}[ 0, \uparrow, +\rangle +  0, \uparrow, -\rangle],$
Phase (I)	$ v_1\rangle = \cos\theta 1, \uparrow, +\rangle + \sin\theta 1, \uparrow, -\rangle,  v_2\rangle = \cos\theta 0, \uparrow, +\rangle + \sin\theta 0, \uparrow, -\rangle,$
Phase (II)	$ v_1\rangle =  1, \uparrow, +\rangle,  v_2\rangle =  0, \uparrow, +\rangle.$
Phase (III)	$ v_1\rangle =  0, \uparrow, +\rangle,  v_2\rangle =  0, \downarrow, +\rangle,$

TABLE III: The different GS configurations which occur at filling  $\nu = -2$ .

Hence, in this phase, cuts along lines of increasing bias  $\Delta_B$ , for any strength of the magnetic field  $B$ , correspond to a rotation of the valley-isospin vector from a configuration in the  $x$ - $y$ -plane to fully aligned along the  $z$ -axis.

Phase (II): within an intermediate range of the bias  $\Delta_B$ , the GS is a fully polarized ferromagnet in spin and valley isospin. The orbital isospin degree of freedom, however, is in an antiferromagnetic configuration yielding zero overall orbital polarization.

Phase (III): in the limit of a sufficiently large bias  $\Delta_B$ , we find the GS to be an antiferromagnet in spin. The valley isospin is fully polarized, whereas the orbital isospin turns out to be fully antiferromagnetically polarized.

At filling factor  $\nu = -2$ , we observe two different types of phase transitions: going from phase (I) to phase (II) is achieved by a smooth rotation of the valley isospin. This is a second order transition. From phase (II) to phase (III), however, the system undergoes jumps in spin and orbital isospin degree of freedom, which characterizes a discontinuous first order phase transition. The critical values of the bias for these transitions read, respectively:

(I)  $\rightarrow$  (II) :

$$\Delta_{B,eff}^{crit} = \frac{-4\alpha d - \Delta_{0000}\ell_B - 2\Delta_{0011}\ell_B - \Delta_{1111}\ell_B + \ell_B X_{0000} + 2\ell_B X_{0011} + \ell_B X_{1111}}{\ell_B(z-2)}. \quad (29)$$

(II)  $\rightarrow$  (III): The GS of phase (II) is lower in energy than the GS of phase (III) up to a critical bias

$$\Delta_{B,eff}^{crit} = \frac{1}{z}(\Delta_{0000} - 2\Delta_{0011} + 2\Delta_{01} - \Delta_{1111} + 2\Delta_Z). \quad (30)$$

### C. Three electrons: $\nu = -1$

When there are three electrons in the system, we find the following GS structure:

Unbiased case ( $\Delta_B \equiv 0$ , evolution as a function of  $B$ ): the GS is a fully polarized spin ferromagnet, while its valley isospin lies in the  $\{x$ - $y$ \}-plane, and the orbital isospin is canted in an orbital coherent phase. The optimal canting angle in orbital space  $\theta_0$  as shown in Fig. 5 varies as a function of  $B$  between  $\theta_0 \rightarrow \frac{\pi}{4}$  at vanishing magnetic field  $B \rightarrow 0$  and  $\theta_0 = \frac{\pi}{2}$  at magnetic field strengths above  $B_{crit} \approx 11.3$  T. It fulfills the relation

$$\cos 2\theta_0 = \frac{-3\Delta_{0000} - 4\Delta_{01} + 3\Delta_{1111} + X_{0000} - X_{1111}}{\Delta_{0000} - 2(\Delta_{0011} + \Delta_{1001}) + \Delta_{1111} + X_{0000} - 2(X_{0011} + X_{1001}) + X_{1111}}. \quad (31)$$

Along the line of zero bias, as a function of increasing magnetic field strength  $B$ , the GS hence undergoes a transition from a canted state in the orbital isospin to a partially polarized state.

Phases (I) and (II): in the regime of very small bias  $\Delta_B$ , we find a rotation of the valley-isospin at either canted or partially aligned orbital isospin, respectively. In both phases (I) and (II) the GS is a fully polarized spin ferromagnet. The valley isospin assumes non-trivial configurations  $0 \leq T_x, T_z \leq 1$ ,  $T_y \equiv 0$ . Phase (I) occurs for sufficiently small values of the magnetic field,  $B < B_{crit}$ ; the corresponding GS is given by an involved superposition of different SP states (cf. table IV) which leads to a non-trivial isospin configuration. In phase (II), however, *i.e.* at field values above the critical magnetic field, we can describe the valley isospin in simple terms with the valley canting angle  $\theta$  as the only parameter, where the optimal angle turns out to be

$$\cos 2\theta_{(II)} = \frac{\Delta_{B,eff}\ell_B}{\alpha d + \ell_B(\Delta_{0000} - X_{0000})}. \quad (32)$$

The orbital isospin in phase (I) is in a canted configuration,  $0 \leq L_x, L_z \leq 1$ ,  $L_y \equiv 0$ , whereas phase (II) is partially polarized in orbital space. Hence, in phase (I) and (II), cuts along lines of increasing bias  $\Delta_B$  for any strength of the magnetic field  $B$  correspond to a rotation of the valley-isospin vector from a configuration in the  $\{x$ - $y$ \}-plane to a state fully aligned along the  $z$ -axis. At the same time, increasing  $B$  at a fixed value of the bias  $\Delta_B$  corresponds to rotating the LL-isospin from a canted configuration in phase (I) to a partly polarized configuration in phase (II).

Phase (III) and (IV): At larger values of the bias  $\Delta_B$  we find pendants of phase (I) and (II), now at polarized configurations of the valley isospin: here, the GS is a fully polarized spin ferromagnet and a partially polarized valley isospin, while the orbital isospin degree of freedom again varies as function of the bias  $\Delta_B$  and the magnetic field strength  $B$ : It is canted for small values of the magnetic field in phase (III) with optimal canting angle

$$\cos 2\theta_{(III)} = \frac{\Delta_{0000} + 2\Delta_{01} - \Delta_{1111} + z\Delta_{B,eff}}{\Delta_{0000} - 2(\Delta_{0011} + \Delta_{1001}) + \Delta_{1111}}, \quad (33)$$

which evolves into the partially polarized phase (IV) above a critical value of the field  $B_{crit}$ . Hence, increasing the magnetic field strength  $B$  corresponds to rotating the orbital isospin from a canted configuration in phase (III) to a partially polarized state in phase (IV). Both the spin and the valley isospin vectors remain constant in these phases for all values of  $\Delta_B$  and  $B$ .

Phase (V): A narrow transition regime is established with complex behavior of the GS configuration. All spin and isospin degrees of freedom take nontrivial values and evolve as functions of  $\Delta_B$  and  $B$ . Exploiting the notation of the states as given in Table IV, we write  $S_z = 1 + \frac{1}{2}(c_1^2 - c_2^2 + c_3^2 - c_4^2)$ ,  $S_x \equiv S_y \equiv 0$ ,  $T_z = 1 - \frac{1}{2}(c_1^2 - c_2^2 + c_3^2 - c_4^2)$ ,  $T_x \equiv T_y \equiv 0$ , and  $L_z = \frac{1}{2}(c_1^2 + c_2^2 - c_3^2 - c_4^2)$ ,  $L_x = -(c_1c_3 + c_2c_4)$ ,  $L_y \equiv 0$ . Within the parameter range of phase (V) one can distinguish between the following regimes: Phase (Va): For  $B < B_{crit}$ , all four entries  $c_i \neq 0$  evolve smoothly as functions of the bias  $\Delta_B$  and the magnetic field strength  $B$ . For increasing  $\Delta_B$  across phase (Va), this leads to smooth evolution of the spin and valley isospins from  $S_z = \frac{3}{2}$  to  $S_z = \frac{1}{2}$  and from  $T_z = \frac{1}{2}$  to  $T_z = \frac{3}{2}$ , respectively, accompanied by kinks in the orbital isospin components which are nonzero within this range:  $0 < L_z < \frac{1}{2}$  and  $0 < L_x < \frac{1}{2}$ . Phases (Vb) and (Vc): For  $B > B_{crit}$ , two competing transitions occur within the parameter range of phase (V): there is a smooth evolution of  $S_z$  and  $T_z$  as in the former case. It is governed by smoothly evolving entries  $c_1$  and  $c_2$  while  $c_3 \equiv c_4 \equiv 0$  (so that  $L_x \equiv 0$  and  $L_z \equiv \frac{1}{2}$  fixed by normalization). At a sufficiently high value of  $\Delta_B$ , eventually,  $c_4$  jumps to a nonzero value, thereby inducing nonzero values of  $L_z$  and  $L_x$  and nontrivial evolution of all spin and isospin degrees of freedom. Phase (VI) occupies a wide parameter range including all magnetic field strengths and intermediate values of the bias  $\Delta_B$ . While the spin is partially polarized and the valley isospin is fully polarized, the orbital isospin is in a canted configuration, assuming the optimal canting angle

$$\cos 2\theta_{(VI)} = \frac{\Delta_{0000} + 2\Delta_{01} - \Delta_{1111} - z\Delta_{B,eff}}{\Delta_{0000} - 2(\Delta_{0011} + \Delta_{1001}) + \Delta_{1111}}. \quad (34)$$

Hence, for any value of the magnetic field  $B$ , with rising bias  $\Delta_B$  the orbital isospin performs a rotation to a partially antiferromagnetically polarized configuration:  $\mathbf{L} \rightarrow -\frac{1}{2}\mathbf{e}_z$ .

Phase (VII): For sufficiently large values of the bias, the GS phase eventually reaches a configuration which is partially polarized in spin, fully polarized in the valley isospin, and partially antiferromagnetically-polarized in the orbital isospin degree of freedom. Except for the transition regime of phase (V) described above, all phase transitions of the  $\nu = -1$  phase diagram go along with smooth rotations of the respective isospin vectors and therefore are of second order. The most prominent transitions occur at the following critical values of the bias:

(II)  $\rightarrow$  (IV):

$$\Delta_{B,eff}^{crit} = \frac{\alpha d + \Delta_{0000}\ell_B - \ell_B X_{0000}}{\ell_B}, \quad (35)$$

(III)  $\rightarrow$  (IV):

$$\Delta_{B,eff}^{crit} = -\frac{2}{z}(\Delta_{0011} + \Delta_{01} + \Delta_{1001} - \Delta_{1111}), \quad (36)$$

(IV)  $\rightarrow$  (Vb):

$$\Delta_{B,eff}^{crit} = \frac{-\alpha d + \Delta_{1111}\ell_B - \Delta_Z\ell_B - \ell_B X_{1111}}{\ell_B(z-1)}, \quad (37)$$

(VI)  $\rightarrow$  (VII):

$$\Delta_{B,eff}^{crit} = \frac{2}{z}(\Delta_{0000} - \Delta_{0011} + \Delta_{01} - \Delta_{1001}). \quad (38)$$

$\Delta_B = 0$	$ v_1\rangle = -\frac{1}{\sqrt{2}}[ 1, \uparrow, +\rangle +  1, \uparrow, -\rangle],  v_2\rangle = \frac{1}{\sqrt{2}}[ 0, \uparrow, +\rangle +  0, \uparrow, -\rangle],$ $ v_3\rangle = -\frac{1}{\sqrt{2}}\sin\theta[ 1, \uparrow, +\rangle -  1, \uparrow, -\rangle] - \frac{1}{\sqrt{2}}\cos\theta[ 0, \uparrow, +\rangle -  0, \uparrow, -\rangle],$
Phase (I)	$ v_1\rangle = -a_1 1, \uparrow, +\rangle - a_2 1, \uparrow, -\rangle + b_1 0, \uparrow, +\rangle + b_2 0, \uparrow, -\rangle,$ $ v_2\rangle = b_1 1, \uparrow, +\rangle + b_2 1, \uparrow, -\rangle + a_1 0, \uparrow, +\rangle + a_2 0, \uparrow, -\rangle,$ $ v_3\rangle = c_1 1, \uparrow, +\rangle - c_2 1, \uparrow, -\rangle - c_3 0, \uparrow, +\rangle + c_4 0, \uparrow, -\rangle,$
Phase (II)	$ v_1\rangle = -\cos\theta 1, \uparrow, +\rangle - \sin\theta 1, \uparrow, -\rangle,  v_2\rangle = \cos\theta 0, \uparrow, +\rangle + \sin\theta 0, \uparrow, -\rangle,$ $ v_3\rangle = \sin\theta 1, \uparrow, +\rangle - \cos\theta 1, \uparrow, -\rangle,$
Phase (III)	$ v_1\rangle =  1, \uparrow, +\rangle,  v_2\rangle =  0, \uparrow, +\rangle,  v_3\rangle = \cos\theta 1, \uparrow, -\rangle + \sin\theta 0, \uparrow, -\rangle$
Phase (IV)	$ v_1\rangle =  1, \uparrow, +\rangle,  v_2\rangle =  0, \uparrow, +\rangle,  v_3\rangle =  1, \uparrow, -\rangle$
Phase (V)	$ v_1\rangle =  1, \uparrow, +\rangle,  v_2\rangle =  0, \uparrow, +\rangle,$ $ v_3\rangle = c_1 1, \uparrow, -\rangle + c_2 1, \downarrow, +\rangle - c_3 0, \uparrow, -\rangle - c_4 0, \downarrow, +\rangle$
Phase (VI)	$ v_1\rangle =  1, \uparrow, +\rangle,  v_2\rangle =  0, \uparrow, +\rangle,  v_3\rangle = \cos\theta 1, \downarrow, +\rangle + \sin\theta 0, \downarrow, +\rangle$
Phase (VII)	$ v_1\rangle =  1, \uparrow, +\rangle,  v_2\rangle =  0, \uparrow, +\rangle,  v_3\rangle =  0, \downarrow, +\rangle$

TABLE IV: The possible GS configurations identified for the phase diagram at filling factor  $\nu = -1$ .

#### D. Four electrons: $\nu = 0$

The bilayer system is charge neutral when there are four electrons per state occupying exactly half of the states within the octet. For this configuration of half filling we find the following different GS phases:

Phase (I): in the unbiased configuration as well as for sufficiently small values of the bias  $\Delta_B$ , the GS is a fully polarized spin ferromagnet, while it is an antiferromagnet both in valley and in orbital space, leading to vanishing overall valley and orbital polarization. Phase (II): for all magnetic field strengths and in an intermediate regime of the bias, the spin and the valley isospin undergo evolution as functions of  $\Delta_B$  and  $B$  as a function of one angle  $\theta$ , which minimizes the energy for

$$\cos 2\theta_{(II)} = \frac{4\alpha d + 2\Delta_Z \ell_B + \Delta_{Beff} \ell_B (z - 2)}{4\alpha d + \ell_B (\Delta_{0000} + 2\Delta_{0011} + \Delta_{1111} - X_{0000} - 2X_{0011} - X_{1111})}. \quad (39)$$

In orbital space, the state is an antiferromagnet, with zero orbital polarization. Hence, for a given value of the magnetic field  $B$ , upon increasing the bias  $\Delta_B$  over the parameter range of phase (II), the total spin evolves from a fully aligned state to a state with zero total spin, while contrarily the total valley isospin evolves from zero to a fully polarized valley ferromagnet state:  $\mathbf{S} = 2\mathbf{e}_z \rightarrow \mathbf{S} \equiv 0, \mathbf{T} \equiv 0 \rightarrow \mathbf{T} = 2\mathbf{e}_z$ .

Phase (III): For sufficiently large values of the bias  $\Delta_B$  the GS assumes antiferromagnetic order in both spin space and in the space of the orbital isospin, while being a fully polarized ferromagnet in valley space. The transitions between the different GS phases of  $\nu = 0$  are all characterized by smooth rotations of the isospin degrees of freedom indicating continuous second order transitions. We give the critical values of the bias at which these phase transitions occur:

(I)  $\rightarrow$  (II):

$$\Delta_{B,eff}^{crit} = \frac{\Delta_{0000} + 2\Delta_{0011} + \Delta_{1111} - 2\Delta_Z - X_{0000} - 2X_{0011} - X_{1111}}{z - 2}, \quad (40)$$

(II)  $\rightarrow$  (III) :

$$\Delta_{B,eff}^{crit} = \frac{\ell_B (-\Delta_{0000} - 2\Delta_{0011} - \Delta_{1111} - 2\Delta_Z + X_{0000} + 2X_{0011} + X_{1111}) - 8\alpha d}{\ell_B (z - 2)}. \quad (41)$$

#### E. Five electrons: $\nu = 1$

For the case of five electrons we identify the following GS structure:

Unbiased case ( $\Delta_B \equiv 0$ , evolution as a function of  $B$ ): At zero bias, we find a GS configuration in which the spin is partially polarized, while the valley isospin vector lies in the  $\{xy\}$ -plane. The orbital isospin assumes a canted configuration, thus exhibiting non-trivial orbital coherence. The optimal canting angle in orbital space  $\theta_0$ , as shown

Phase (I)	$ v_1\rangle =  1, \uparrow, +\rangle,  v_2\rangle =  1, \uparrow, -\rangle,  v_3\rangle =  0, \uparrow, +\rangle,  v_4\rangle =  0, \uparrow, -\rangle$
Phase (II)	$ v_1\rangle =  1, \uparrow, +\rangle,  v_2\rangle = \cos\theta 1, \uparrow, -\rangle + \sin\theta 1, \downarrow, +\rangle,$ $ v_3\rangle =  0, \uparrow, +\rangle,  v_4\rangle = \cos\theta 0, \uparrow, -\rangle + \sin\theta 0, \downarrow, +\rangle$
Phase (III)	$ v_1\rangle =  1, \uparrow, +\rangle,  v_2\rangle =  1, \downarrow, +\rangle,  v_3\rangle =  0, \uparrow, +\rangle,  v_4\rangle =  0, \downarrow, +\rangle$

TABLE V: The three different GS we identified for the phase diagram of  $\nu = 0$ .

in Fig. 5, varies as a function of  $B$  between  $\theta_0 \rightarrow \frac{\pi}{4}$  at vanishing magnetic field  $B \rightarrow 0$  and  $\theta_0 = 0$  above a critical value  $B_{crit} \approx 11$  T. This angle fulfills the relation

$$\cos\theta_0 = \frac{\sqrt{\Delta_{0000} - \Delta_{0011} + 2\Delta_{01} - \Delta_{1001} + X_{0000} - X_{0011} - X_{1001}}}{\sqrt{\Delta_{0000} - 2\Delta_{0011} - 2\Delta_{1001} + \Delta_{1111} + X_{0000} - 2X_{0011} - 2X_{1001} + X_{1111}}}. \quad (42)$$

Along the line of zero bias, as a function of increasing magnetic field strength  $B$ , the GS hence undergoes a transition from a canted state in the orbital isospin to a partially polarized state.

Phases (I) and (II): at small values of the bias  $\Delta_B$ , these phases are in a partially polarized spin state, while the valley isospin takes non-trivial values  $0 \leq T_x, T_z \leq 1$ . Meanwhile, the orbital isospin is either in canted configuration with  $0 \leq L_x, L_z \leq 1$  (phase I, for sufficiently small values of the magnetic field) or is partially polarized (phase II, above some critical magnetic field strength). The former case being more involved, in the latter phase (II) we find a single parameter dependence of the states' configuration with one optimal angle  $\theta$  determined by

$$\cos 2\theta_{(II)} = \frac{\Delta_{B,eff}\ell_B(z-1)}{\ell_B(X_{1111} - \Delta_{1111}) - \alpha d}, \quad (43)$$

governing the canting in valley space. Hence, in phase (I) and (II), cuts along lines of increasing bias  $\Delta_B$  for any strength of the magnetic field  $B$  correspond to a rotation of the valley-isospin vector from a configuration in the  $\{x-y\}$ -plane to a state aligned along the  $z$ -axis:  $\mathbf{T} = \frac{1}{2}\mathbf{e}_x \rightarrow \mathbf{T} = \frac{1}{2}\mathbf{e}_z$ . Meanwhile, increasing  $B$  at fixed value of the bias  $\Delta_B$  corresponds to rotating the orbital isospin from a canted configuration in phase (I) to a partially polarized configuration in phase (II).

Phase (III) and (IV): at larger values of the bias  $\Delta_B$ , similar behavior as in phases (I) and (II) translates into valley polarized phases: we find the GS to be partially polarized both in spin space and in the space of the valley isospin, while the orbital isospin is either canted (below a critical magnetic field in phase III) or partially polarized (for sufficiently large magnetic field values in phase IV). The optimal canted angle of the orbital isospin is determined by

$$\cos 2\theta_{(III)} = \frac{\Delta_{0000} + 2\Delta_{01} - \Delta_{1111} - z\Delta_{B,eff}}{\Delta_{0000} - 2(\Delta_{0011} + \Delta_{1001}) + \Delta_{1111}}. \quad (44)$$

This angle varies as function of the bias  $\Delta_B$  and the magnetic field strength  $B$ . At any value of  $\Delta_B$ , when  $B$  increases, the angle rotates until it reaches zero, leading to the partially polarized orbital state. Hence, increasing the magnetic field strength  $B$  corresponds to rotating the orbital isospin from a canted configuration in phase (III) to a partially polarized state in phase (IV). Both the spin and the valley isospin vectors remain constant in these phases for all values of  $\Delta_B$  and  $B$ .

Phase (V): within a narrow range of the bias  $\Delta_B$ , there is an intermediate transition regime: We find a complex GS structure in which all the spin and isospin degrees of freedom take nontrivial values and evolve as functions of  $\Delta_B$  and the magnetic field strength  $B$ . With the notation of the states used in Table VI, the spin and isospin configurations read  $S_z = 1 + \frac{1}{2}(a_1^2 - a_2^2 + b_1^2 - b_2^2 + c_1^2 - c_2^2 + c_3^2 - c_4^2)$ ,  $S_x \equiv S_y \equiv 0$ ,  $T_z = 1 - \frac{1}{2}(a_1^2 - a_2^2 + b_1^2 - b_2^2 + c_1^2 - c_2^2 + c_3^2 - c_4^2)$ ,  $T_x \equiv T_y \equiv 0$ , and  $L_z = \frac{1}{2}(a_1^2 + a_2^2 - b_1^2 - b_2^2 + c_1^2 + c_2^2 - c_3^2 - c_4^2)$ ,  $L_x = c_1c_3 + c_2c_4$ ,  $L_y \equiv 0$ .

Cuts of increasing bias  $\Delta_B$  at fixed  $B$  may exhibit three different types of behavior depending on the value of  $B$ :

(Va): For small  $B$ , the phase (Va) is located between the phases (III) and (VI): in both these phases, the orbital isospin is neither zero nor fully polarized, exhibiting non-zero value  $L_x \neq 0$ . Phase (Va) now smoothly connects between these two phases with all four entries  $a_i \neq 0$ ,  $b_i \neq 0$ , and  $c_i \neq 0$  evolving smoothly as functions of the bias  $\Delta_B$  and the magnetic field strength  $B$ . For increasing  $\Delta_B$  across phase (Va), this leads to smooth evolution of the spin and valley isospins from  $S_z = \frac{3}{2}$  to  $S_z = \frac{1}{2}$  and from  $T_z = \frac{1}{2}$  to  $T_z = \frac{3}{2}$ , respectively, accompanied by kinks in the orbital isospin components being nonzero  $0 < L_z < \frac{1}{2}$  and  $0 < L_x < \frac{1}{2}$ .

(Vb): For an intermediate value of  $B$ , the phase (Vb) emerges between the phases (III) and (VII). In the former, the orbital isospin is not fully polarized with  $L_x \neq 0$ , whereas in the latter only the x-component is nonzero:  $L_z = \frac{1}{2}$  and  $L_x \equiv L_y \equiv 0$ . This transition is accomplished within phase (Vb) by first a sudden jump of the orbital isospin

$L_x \rightarrow 0$ ,  $L_z \rightarrow \frac{1}{2}$  as the coefficients  $c_3$  and  $c_4$  suddenly jump to zero; Subsequently, the smooth rotations of the spin and the valley isospin degrees of freedom are governed by the remaining coefficients  $a_i$  and  $b_i$  evolving smoothly.

(Vc): For large enough values of the magnetic field, the phase (Vc) is located between the phases (IV) and (VII) - both these phases exhibit the same configuration of the orbital isospin degree of freedom:  $\mathbf{L} = \frac{1}{2}\mathbf{e}_z$ . Here, the coefficients  $c_i$  are zero throughout the phase (Vc):  $c_1 \equiv c_2 \equiv 0$ . The orbital isospin therefore remains constant within this regime. The remaining coefficients  $a_i$  and  $b_i$  evolve smoothly as functions of  $\Delta_B$  and  $B$ , smooth rotations  $S_z = \frac{3}{2} \rightarrow S_z = \frac{1}{2}$   $T_z = \frac{1}{2} \rightarrow T_z = \frac{3}{2}$  across phase (Vc).

Phase (VI) and (VII): For sufficiently large values of the bias  $\Delta_B$ , we observe GS structures akin to those of phases (III) and (IV), but here at full valley polarization: At partially polarized spin and fully valley polarized isospin, the orbital isospin rotates from a canted position we call phase (VI) at sufficiently small magnetic fields to a partially polarized state, i.e., phase (VII), above a certain critical magnetic field strength. The optimal orbital canting angle hereby is determined by

$$\cos 2\theta_{(VI)} = \frac{\Delta_{0000} + 2\Delta_{01} - \Delta_{1111} + z\Delta_{B\text{eff}}}{\Delta_{0000} - 2(\Delta_{0011} + \Delta_{1001}) + \Delta_{1111}}. \quad (45)$$

Hence, for any value of the magnetic field  $B$ , with rising bias  $\Delta_B$  the orbital isospin performs a rotation to a configuration aligned along the  $z$ -axis:  $\mathbf{L} \rightarrow \frac{1}{2}\mathbf{e}_z$ . At sufficiently large values of the bias, phase (VII) eventually is fully polarized along the  $z$ -axis in valley isospin, and partially polarized in the spin and orbital isospin degree of freedom.

Except for the more complicated transition regime within phase (V), all phase transitions observed for the  $\nu = 1$  state are of continuous second order nature. We compute the critical values of the bias for these transitions, respectively:

(II)  $\rightarrow$  (IV):

$$\Delta_{B,\text{eff}}^{\text{crit}} = \frac{-\alpha d - \Delta_{1111}\ell_B + \ell_B X_{1111}}{\ell_B(z-1)}, \quad (46)$$

(III)  $\rightarrow$  (IV):

$$\Delta_{B,\text{eff}}^{\text{crit}} = \frac{2(\Delta_{0011} + \Delta_{01} + \Delta_{1001} - \Delta_{1111})}{z}, \quad (47)$$

(IV)  $\rightarrow$  (Vc):

$$\Delta_{B,\text{eff}}^{\text{crit}} = \frac{\alpha d - \Delta_{0000}\ell_B + \Delta_Z\ell_B + \ell_B X_{0000}}{\ell_B}, \quad (48)$$

(Vc)  $\rightarrow$  (VII):

$$\Delta_{B,\text{eff}}^{\text{crit}} = \frac{3\alpha d + \Delta_{0000}\ell_B + \Delta_Z\ell_B - \ell_B X_{0000}}{\ell_B}, \quad (49)$$

(VI)  $\rightarrow$  (VII):

$$\Delta_{B,\text{eff}}^{\text{crit}} = -\frac{2(\Delta_{0011} + \Delta_{01} + \Delta_{1001} - \Delta_{1111})}{z}. \quad (50)$$

## F. Six electrons: $\nu = 2$

If there are six electrons occupying octet states, the structure we find for the GS is the following:

Phase (I): In the regime of sufficiently small bias, we observe a GS which is partially polarized in spin and exhibits valley coherence in a valley canted phase where the optimal valley canting angle is given by

$$\cos 2\theta_{(I)} = -\frac{\Delta_{B,\text{eff}}\ell_B(z-2)}{\ell_B(-\Delta_{0000} - 2\Delta_{0011} - \Delta_{1111} + X_{0000} + 2X_{0011} + X_{1111}) - 4\alpha d}. \quad (51)$$

The orbital order is antiferromagnetic, which leads to vanishing overall orbital polarization. Hence, in phase (I), cuts along lines of increasing bias  $\Delta_B$  for any strength of the magnetic field  $B$  correspond to a rotation of the valley-isospin vector from a configuration in the  $\{x-y\}$ -plane to a state partially polarized along the  $z$ -axis:  $\mathbf{T} = \mathbf{e}_x \rightarrow \mathbf{T} = \mathbf{e}_z$ .

$\Delta_B = 0$	$ v_1\rangle =  1, \uparrow, +\rangle,  v_2\rangle =  1, \uparrow, -\rangle,  v_3\rangle =  0, \uparrow, +\rangle,  v_4\rangle =  0, \uparrow, -\rangle,$ $ v_5\rangle = \frac{1}{\sqrt{2}} \cos \theta \left[  1, \downarrow, +\rangle +  1, \downarrow, -\rangle \right] - \frac{1}{\sqrt{2}} \sin \theta \left[  0, \downarrow, +\rangle +  0, \downarrow, -\rangle \right]$
Phase (I)	$ v_1\rangle =  1, \uparrow, +\rangle,  v_2\rangle =  1, \uparrow, -\rangle,  v_3\rangle =  0, \uparrow, +\rangle,  v_4\rangle =  0, \uparrow, -\rangle,$ $ v_5\rangle = a_1  1, \downarrow, +\rangle + a_2  1, \downarrow, -\rangle - a_3  0, \downarrow, +\rangle - a_4  0, \downarrow, -\rangle$
Phase (II)	$ v_1\rangle =  1, \uparrow, +\rangle,  v_2\rangle =  1, \uparrow, -\rangle,  v_3\rangle =  0, \uparrow, +\rangle,  v_4\rangle =  0, \uparrow, -\rangle,  v_5\rangle = \cos \theta  1, \downarrow, +\rangle + \sin \theta  1, \downarrow, -\rangle$
Phase (III)	$ v_1\rangle =  1, \uparrow, +\rangle,  v_2\rangle =  1, \uparrow, -\rangle,  v_3\rangle =  0, \uparrow, +\rangle,  v_4\rangle =  0, \uparrow, -\rangle,  v_5\rangle = \cos \theta  1, \downarrow, +\rangle + \sin \theta  0, \downarrow, +\rangle$
Phase (IV)	$ v_1\rangle =  1, \uparrow, +\rangle,  v_2\rangle =  1, \uparrow, -\rangle,  v_3\rangle =  0, \uparrow, +\rangle,  v_4\rangle =  0, \uparrow, -\rangle,  v_5\rangle =  1, \downarrow, +\rangle$
Phase (V)	$ v_1\rangle =  1, \uparrow, +\rangle,  v_2\rangle = a_1  1, \uparrow, -\rangle + a_2  1, \downarrow, +\rangle,  v_3\rangle =  0, \uparrow, +\rangle,  v_4\rangle = b_1  0, \uparrow, -\rangle + b_2  0, \downarrow, +\rangle,$ $ v_5\rangle = c_1  1, \uparrow, -\rangle + c_2  1, \downarrow, +\rangle + c_3  0, \uparrow, -\rangle + c_4  0, \downarrow, +\rangle$
Phase (VI)	$ v_1\rangle =  1, \uparrow, +\rangle,  v_2\rangle =  1, \downarrow, +\rangle,  v_3\rangle =  0, \uparrow, +\rangle,  v_4\rangle =  0, \downarrow, +\rangle,  v_5\rangle = \cos \theta  1, \uparrow, -\rangle + \sin \theta  0, \uparrow, -\rangle$
Phase (VII)	$ v_1\rangle =  1, \uparrow, +\rangle,  v_2\rangle =  1, \downarrow, +\rangle,  v_3\rangle =  0, \uparrow, +\rangle,  v_4\rangle =  0, \downarrow, +\rangle,  v_5\rangle =  1, \uparrow, -\rangle$

TABLE VI: GS configurations identified in the phase diagram for filling factor  $\nu = 1$ .

$\Delta_B \equiv 0$	$ v_1\rangle =  1, \uparrow, +\rangle,  v_2\rangle =  1, \uparrow, -\rangle,  v_3\rangle =  0, \uparrow, +\rangle,  v_4\rangle =  0, \uparrow, -\rangle,$ $ v_5\rangle = \frac{1}{\sqrt{2}} \left[  1, \downarrow, +\rangle +  1, \downarrow, -\rangle \right],  v_6\rangle = \frac{1}{\sqrt{2}} \left[  0, \downarrow, +\rangle +  0, \downarrow, -\rangle \right]$
Phase (I)	$ v_1\rangle =  1, \uparrow, +\rangle,  v_2\rangle =  1, \uparrow, -\rangle,  v_3\rangle =  0, \uparrow, +\rangle,  v_4\rangle =  0, \uparrow, -\rangle,$ $ v_5\rangle = \sin \theta  1, \downarrow, +\rangle + \cos \theta  1, \downarrow, -\rangle,  v_6\rangle = \sin \theta  0, \downarrow, +\rangle + \cos \theta  0, \downarrow, -\rangle$
Phase (II)	$ v_1\rangle =  1, \uparrow, +\rangle,  v_2\rangle =  1, \uparrow, -\rangle,  v_3\rangle =  0, \uparrow, +\rangle,  v_4\rangle =  0, \uparrow, -\rangle,  v_5\rangle =  1, \downarrow, +\rangle,  v_6\rangle =  0, \downarrow, +\rangle$
Phase (III)	$ v_1\rangle =  1, \uparrow, +\rangle,  v_2\rangle =  1, \uparrow, -\rangle,  v_3\rangle =  0, \uparrow, +\rangle,  v_4\rangle =  1, \downarrow, -\rangle,  v_5\rangle =  1, \downarrow, +\rangle,  v_6\rangle =  0, \downarrow, +\rangle$

TABLE VII: The different possible GS configurations we observed at filling factor  $\nu = 2$ .

Phase (II): For larger values of the bias  $\Delta_B$ , we observe an intermediate regime in which the GS exhibits partial polarization both in the spin and the valley isospin degree of freedom and antiferromagnetic ordering in the orbital isospin. Hence, the GS is a partially aligned spin and valley ferromagnet over a broad parameter range.

Phase (III): When the system is biased sufficiently strongly, we find the GS to be a polarized state both for the valley and the orbital isospin. Meanwhile, due to antiferromagnetic ordering of the spin degree of freedom, the overall spin polarization vanishes. This phase for large values of the bias  $\Delta_B$  is established for all magnetic field strengths. For the system at filling  $\nu = 2$  we identify two different types of phase transitions as functions of  $\Delta_B$  and  $B$ : The small bias transition (I) to (II) comes with a smooth rotation of the valley isospin and therefore is of continuous second order. For larger bias, however, the system jumps from phase (II) to phase (III) in a discontinuous fashion characterizing a first order transition. We give the values of the critical bias at which these phase transitions occur:

(I)  $\rightarrow$  (II):

$$\Delta_{B,eff}^{crit} = \frac{\ell_B(X_{0000} + 2X_{0011} + X_{1111} - \Delta_{0000} - 2\Delta_{0011} - \Delta_{1111}) - 4\alpha d}{\ell_B(z - 2)}, \quad (52)$$

(II)  $\rightarrow$  (III): Phase (II) is energetically favorable over phase (III) up to a the critical bias

$$\Delta_{B,eff}^{crit} = \frac{-\Delta_{0000} - 2\Delta_{0011} - 2\Delta_{01} + \Delta_{1111} + 2\Delta_Z}{z}. \quad (53)$$

### G. Seven electrons: $\nu = 3$

With only one hole in the octet, the GS exhibit the following structure: in the unbiased case ( $\Delta_B \equiv 0$ , evolution as a function of  $B$ ), we find a partially spin polarized GS, while the valley isospin is aligned along the  $x$ -axis. The state exhibits orbital coherence as the orbital isospin is in a canted configuration, where the optimal angle  $\theta_0$  varies as a function of  $B$  between  $\theta_0 \rightarrow \frac{\pi}{4}$  at vanishing magnetic field  $B \rightarrow 0$  and  $\theta_0 = \frac{\pi}{2}$  at sufficiently high magnetic field strengths above a certain critical value  $B_{crit} \approx 11.3$  T. It fulfills the relation

$$\cos 2\theta_0 = \frac{-3\Delta_{0000} - 4\Delta_{01} + 3\Delta_{1111} + X_{0000} - X_{1111}}{\Delta_{0000} - 2\Delta_{0011} - 2\Delta_{1001} + \Delta_{1111} + X_{0000} - 2X_{0011} - 2X_{1001} + X_{1111}}. \quad (54)$$

Along the line of zero bias, as a function of increasing magnetic field strength  $B$  the GS hence undergoes a transition from a canted state in the orbital isospin to a partially aligned state.

Phases (I) and (II): in this regime of sufficiently weak bias  $\Delta_B$ , the GS has partial polarization in spin space, while the valley isospin undergoes a rotation and therefore takes nontrivial values  $0 \leq T_x, T_z \leq \frac{1}{2}$ . Meanwhile, the orbital isospin is either canted with  $0 \leq L_x, L_z \leq \frac{1}{2}$  for small magnetic field strengths in phase (I), or partially polarized in phase (II) at sufficiently large magnetic fields. While the dependencies of the isospins in phase (I) being more involved, we can express the valley isospin in phase (II) in terms of one valley tilting angle for which the optimal configuration is determined by

$$\cos 2\theta_{(II)} = \frac{\Delta_{B,eff}\ell_B}{\alpha d + \ell_B(\Delta_{0000} - X_{0000})}. \quad (55)$$

Hence, in phase (I) and (II), cuts along lines of increasing bias  $\Delta_B$  for any strength of the magnetic field  $B$  correspond to a rotation of the valley isospin vector from a configuration in the  $\{x-y\}$ -plane to a state aligned along the  $z$ -axis:  $\mathbf{T} = \frac{1}{2}\mathbf{e}_x \rightarrow \mathbf{T} = \frac{1}{2}\mathbf{e}_z$ . At the same time, increasing  $B$  at a fixed value of the bias  $\Delta_B$  corresponds to rotating the orbital isospin from a canted configuration in phase (I) to an aligned configuration,  $\mathbf{L} = \frac{1}{2}\mathbf{e}_z$  in phase (II).

Phase (III): at small magnetic fields and large values of the bias, the spin and the valley isospin degree of freedom are equally partially polarized, while the orbital isospin undergoes a rotation through a canted state, thereby exhibiting nontrivial orbital coherence. The optimal angle in orbital space is determined by

$$\cos 2\theta_{(III)} = \frac{\Delta_{0000} + 2\Delta_{01} - \Delta_{1111} + z\Delta_{B,eff}}{\Delta_{0000} - 2(\Delta_{0011} + \Delta_{1001}) + \Delta_{1111}}, \quad (56)$$

varying as function of the bias  $\Delta_B$  and the magnetic field strength  $B$ .

Phase (IV): when both magnetic field strength  $B$  and bias  $\Delta_B$  are sufficiently large, the GS adopts a configuration in which all spin and isospin degrees of freedom are equally partially polarized.

All the phase transitions for filling factor  $\nu = 3$  are continuous second order transitions, which occur via smooth rotations of the respective isospin degrees of freedom. The critical values of the bias for these transitions are given by (II)  $\rightarrow$  (IV):

$$\Delta_{B,eff}^{crit} = \frac{\alpha d}{\ell_B} + \Delta_{0000} - X_{0000}, \quad (57)$$

(III)  $\rightarrow$  (IV):

$$\Delta_{B,eff}^{crit} = -\frac{2(\Delta_{0011} + \Delta_{01} + \Delta_{1001} - \Delta_{1111})}{z}. \quad (58)$$

## IV. COMPARATIVE DESCRIPTION

### A. General features

The phase diagrams of Fig. 2 displaying the spin and isospin configurations as functions of  $\Delta_B$  and  $B$  share some common features for all filling factors  $\nu \in [-3, 3]$ . In general, we observe many different spin and isospin structures: Among these, the valley and the orbital isospin can be in canted configurations, thus exhibiting non-trivial coherence. In Fig. 2, the regions where such phases occur are drawn in bordeaux, pink, turquoise, yellow, or orange, respectively. The spin and isospin configurations for all the different possible phases are summarized in Tables IX and X.

The unbiased system  $\Delta_B \equiv 0$  is spin polarized for all values of the filling factor. This also remains true for sufficiently small values of the bias in every case (in Fig. 2, all phases except the blue or green ones at even filling factors). In the opposite limit of large bias, valley polarization emerges for all  $\nu$  (blue or green regions in Fig. 2). Qualitatively, this is in accordance with experimental<sup>3</sup> as well as previous theoretical<sup>19</sup> investigations which suggest an evolution towards a valley polarized state with increasing bias. The values of the critical bias and the critical magnetic field strength below (above) which the system is spin (valley) polarized, however, differ for different values of  $\nu$ . Furthermore, it depends on the filling factor whether the respective polarized phase formed in these two limits is partially polarized or fully polarized in spin or valley space.

$\Delta_B = 0$	$ v_1\rangle =  1, \uparrow, +\rangle,  v_2\rangle =  1, \uparrow, -\rangle,  v_3\rangle =  0, \uparrow, +\rangle,  v_4\rangle =  0, \uparrow, -\rangle,$ $ v_5\rangle = \frac{1}{\sqrt{2}} \cos \theta \left[  1, \downarrow, +\rangle +  1, \downarrow, -\rangle \right] + \frac{1}{\sqrt{2}} \sin \theta \left[  0, \downarrow, +\rangle +  0, \downarrow, -\rangle \right],$ $ v_6\rangle = \frac{1}{\sqrt{2}} \sin \theta \left[  1, \downarrow, +\rangle +  1, \downarrow, -\rangle \right] - \frac{1}{\sqrt{2}} \cos \theta \left[  0, \downarrow, +\rangle +  0, \downarrow, -\rangle \right],$ $ v_7\rangle = \frac{1}{\sqrt{2}} \sin \theta \left[  1, \downarrow, +\rangle -  1, \downarrow, -\rangle \right] + \frac{1}{\sqrt{2}} \cos \theta \left[  0, \downarrow, +\rangle -  0, \downarrow, -\rangle \right]$
Phase (I)	$ v_1\rangle =  1, \uparrow, +\rangle,  v_2\rangle =  1, \uparrow, -\rangle,  v_3\rangle =  0, \uparrow, +\rangle,  v_4\rangle =  0, \uparrow, -\rangle,$ $ v_5\rangle = -a_1 1, \downarrow, +\rangle + a_2 1, \downarrow, -\rangle - a_3 0, \downarrow, +\rangle + a_4 0, \downarrow, -\rangle,$ $ v_6\rangle = a_3 1, \downarrow, +\rangle - a_4 1, \downarrow, -\rangle - a_1 0, \downarrow, +\rangle + a_2 0, \downarrow, -\rangle,$ $ v_7\rangle = a_4 1, \downarrow, +\rangle + a_3 1, \downarrow, -\rangle + a_2 0, \downarrow, +\rangle + a_1 0, \downarrow, -\rangle$
Phase (II)	$ v_1\rangle =  1, \uparrow, +\rangle,  v_2\rangle =  1, \uparrow, -\rangle,  v_3\rangle =  0, \uparrow, +\rangle,  v_4\rangle =  0, \uparrow, -\rangle,$ $ v_5\rangle = -\cos \theta  0, \downarrow, +\rangle + \sin \theta  0, \downarrow, -\rangle,  v_6\rangle = \cos \theta  1, \downarrow, +\rangle - \sin \theta  1, \downarrow, -\rangle,$ $ v_7\rangle = \sin \theta  1, \downarrow, +\rangle + \cos \theta  1, \downarrow, -\rangle$
Phase (III)	$ v_1\rangle =  1, \uparrow, +\rangle,  v_2\rangle =  1, \uparrow, -\rangle,  v_3\rangle =  0, \uparrow, +\rangle,  v_4\rangle =  0, \uparrow, -\rangle,$ $ v_5\rangle =  1, \downarrow, +\rangle,  v_6\rangle =  0, \downarrow, +\rangle,  v_7\rangle = \cos \theta  1, \downarrow, -\rangle + \sin \theta  0, \downarrow, -\rangle$
Phase (IV)	$ v_1\rangle =  1, \uparrow, +\rangle,  v_2\rangle =  1, \uparrow, -\rangle,  v_3\rangle =  0, \uparrow, +\rangle,  v_4\rangle =  0, \uparrow, -\rangle,$ $ v_5\rangle =  1, \downarrow, +\rangle,  v_6\rangle =  0, \downarrow, +\rangle,  v_7\rangle =  1, \downarrow, -\rangle$

TABLE VIII: The different possible configurations which occur in the  $\nu = 3$  phase diagram.

### B. Odd versus even filling factors

We now compare the behavior of the orbital degree of freedom for the GS phase diagrams obtained at odd filling factors  $\nu = -3, -1, 1, 3$ . For the unbiased system, i.e., along the line of zero bias  $\Delta_B \equiv 0$ , all the systems with  $\nu$  odd undergo a similar evolution of the orbital isospin: at small  $B$ , we find a canted configuration, then with rising  $B$  the orbital isospin rotates smoothly until it reaches a polarized state above some critical magnetic field strength  $B_{crit}$ . For non-zero values of the bias this transition in the orbital configuration is translated in the upper half of each phase diagram: for every odd filling factor, we find a large phase exhibiting orbital coherence at any  $\Delta_B > 0$  (yellow or orange regions in Fig. 2). These orbitally coherent phases then respectively evolve into orbitally polarized configurations (blue or green phases in Fig. 2, respectively) by smooth rotations of the orbital isospin when  $B$  is increased for any  $\Delta_B$  held fix.

For even filling factors  $\nu = -2, 0, 2$ , however, we do not observe any phase with orbital coherence. There is no phase transition as a function of  $B$  along the line of zero bias, but the GS is in a spin polarized configuration with vanishing orbital isospin stable for all  $B$ . Some of the phases at  $\nu$  even carry orbital polarization, *i.e.* the total orbital isospin is of the form  $\mathbf{L} \propto \mathbf{e}_z$  (blue phase at  $\nu = -2$  and green phase at  $\nu = 2$  in Fig. 2). The remaining phases at even fillings show antiferromagnetic orbital order, *i.e.*, the overall orbital polarization vanishes and we find  $\mathbf{L} \equiv 0$ .

### C. Negative against positive filling factors

The most striking feature when comparing negative  $\nu = -3, -2, -1, 0$  (Table IX) to positive filling factors  $\nu = 1, 2, 3$  (Table X) has to do with the orbital polarization. In the limit of large values of the bias  $\Delta_B$ , the system exhibits orbital polarization for all values of the filling factor (in fig. 2, these phases are drawn in blue or in green). For negative filling factors, however, this polarization is negative,  $\mathbf{L} \propto -\mathbf{e}_z$  (blue phases in Fig. 2), whereas the GS for positive filling factors for sufficiently large bias turns out to be positively polarized,  $\mathbf{L} \propto +\mathbf{e}_z$  (green phases in Fig. 2). Physically, this indicates that at negative filling factors, it is energetically favorable to have predominantly the  $n = 0$  orbitals populated, while at higher filling factors the systems prefer to successively populate  $n = 1$  orbitals.

## V. HF RESULTS II: PHYSICAL PROPERTIES OF THE STATES

### A. Octet Polarization, Hund's Rules, Layer Distribution

We first analyze the spin and isospin polarization properties within the octet. For the unbiased case  $\Delta_B \equiv 0$ , dependence on the system's polarization on the filling factor has been studied previously<sup>12</sup>, establishing Hund's rules for the SP level occupation when the states of the octet are gradually filled with electrons. In Fig. 3, we show the



Phase \ $\nu$	-3	-2	-1	0
$\Delta_B \equiv 0$	$\mathbf{S} = \frac{1}{2}\mathbf{e}_z$ $\mathbf{T} = \frac{1}{2}\mathbf{e}_x$ $\mathbf{L} = \frac{1}{2}\sin 2\theta\mathbf{e}_x + \frac{1}{2}\cos 2\theta\mathbf{e}_z$	$\mathbf{S} = \mathbf{e}_z$ $\mathbf{T} = \mathbf{e}_x$ $\mathbf{L} \equiv 0$	$\mathbf{S} = \frac{3}{2}\mathbf{e}_z$ $\mathbf{T} = \frac{1}{2}\mathbf{e}_z$ $\mathbf{L} = \frac{1}{2}\sin 2\theta\mathbf{e}_x - \frac{1}{2}\cos 2\theta\mathbf{e}_z$	$\mathbf{S} = 2\mathbf{e}_z$ $\mathbf{T} \equiv 0$ $\mathbf{L} \equiv 0$
I	$\mathbf{S} = \frac{1}{2}\mathbf{e}_z$ $0 \leq T_z, T_x \leq \frac{1}{2}, T_y \equiv 0$ $0 \leq L_z, L_x \leq \frac{1}{2}, L_y \equiv 0$	$\mathbf{S} = \mathbf{e}_z$ $\mathbf{T} = \sin 2\theta\mathbf{e}_x + \cos 2\theta\mathbf{e}_z$ $\mathbf{L} \equiv 0$	$\mathbf{S} = \frac{3}{2}\mathbf{e}_z$ $0 \leq T_z, T_x \leq \frac{1}{2}, T_y \equiv 0$ $0 \leq L_z, L_x \leq \frac{1}{2}, L_y \equiv 0$	$\mathbf{S} = 2\mathbf{e}_z$ $\mathbf{T} \equiv 0$ $\mathbf{L} \equiv 0$
II	$\mathbf{S} = \frac{1}{2}\mathbf{e}_z$ $\mathbf{T} = \frac{1}{2}\sin 2\theta\mathbf{e}_x - \frac{1}{2}\cos 2\theta\mathbf{e}_z$ $\mathbf{L} = \frac{1}{2}\mathbf{e}_z$	$\mathbf{S} = \mathbf{e}_z$ $\mathbf{T} = \mathbf{e}_z$ $\mathbf{L} \equiv 0$	$\mathbf{S} = \frac{3}{2}\mathbf{e}_z$ $\mathbf{T} = \frac{1}{2}\sin 2\theta\mathbf{e}_x + \frac{1}{2}\cos 2\theta\mathbf{e}_z$ $\mathbf{L} = \frac{1}{2}\mathbf{e}_z$	$\mathbf{S} = 2\cos^2\theta\mathbf{e}_z$ $\mathbf{T} = 2\sin^2\theta\mathbf{e}_z$ $\mathbf{L} \equiv 0$
III	$\mathbf{S} = \frac{1}{2}\mathbf{e}_z$ $\mathbf{T} = \frac{1}{2}\mathbf{e}_z$ $\mathbf{L} = \frac{1}{2}\mathbf{e}_z$	$\mathbf{S} \equiv 0$ $\mathbf{T} = \mathbf{e}_z$ $\mathbf{L} = -\mathbf{e}_z$	$\mathbf{S} = \frac{3}{2}\mathbf{e}_z$ $\mathbf{T} = \frac{1}{2}\mathbf{e}_z$ $\mathbf{L} = \frac{1}{2}\sin 2\theta\mathbf{e}_x + \frac{1}{2}\cos 2\theta\mathbf{e}_z$	$\mathbf{S} \equiv 0$ $\mathbf{T} = 2\mathbf{e}_z$ $\mathbf{L} \equiv 0$
IV	$\mathbf{S} = \frac{1}{2}\mathbf{e}_z$ $\mathbf{T} = \frac{1}{2}\mathbf{e}_z$ $\mathbf{L} = \frac{1}{2}\sin 2\theta\mathbf{e}_x - \frac{1}{2}\cos 2\theta\mathbf{e}_z$	-	$\mathbf{S} = \frac{3}{2}\mathbf{e}_z$ $\mathbf{T} = \frac{1}{2}\mathbf{e}_z$ $\mathbf{L} = \frac{1}{2}\mathbf{e}_z$	-
V	$\mathbf{S} = \frac{1}{2}\mathbf{e}_z$ $\mathbf{T} = \frac{1}{2}\mathbf{e}_z$ $\mathbf{L} = -\frac{1}{2}\mathbf{e}_z$	-	$\frac{1}{2} \leq S_z \leq \frac{3}{2}, S_x \equiv S_y \equiv 0$ $\frac{1}{2} \leq T_z \leq \frac{3}{2}, T_x \equiv T_y \equiv 0$ $0 \leq L_z, L_x \leq \frac{1}{2}, L_y \equiv 0$	-
VI	-	-	$\mathbf{S} = \frac{1}{2}\mathbf{e}_z$ $\mathbf{T} = \frac{3}{2}\mathbf{e}_z$ $\mathbf{L} = \frac{1}{2}\sin 2\theta\mathbf{e}_x + \frac{1}{2}\cos 2\theta\mathbf{e}_z$	-
VII	-	-	$\mathbf{S} = \frac{1}{2}\mathbf{e}_z$ $\mathbf{T} = \frac{3}{2}\mathbf{e}_z$ $\mathbf{L} = -\frac{1}{2}\mathbf{e}_z$	-

TABLE IX: Spin and isospin properties of the different phases observed for negative filling factors.

pseudospin polarizations for  $B = 15$  T and three bias values  $\Delta_B = 0$  meV,  $\Delta_B = 50$  meV, and  $\Delta_B = 400$  meV. For the unbiased case,  $\Delta_B \equiv 0$ , we recover the results of Barlas et al.<sup>12</sup>. First the real spin degree of freedom is polarized. Second, under the restrictions imposed by the spin configuration, the polarization of the valley isospin and third the polarization of the orbital isospin is maximized to the greatest possible extent. This behavior is shown in the upper plot of Fig. 3. The examples at non-zero values of the bias,  $\Delta_B > 0$ , (central and lower plot of Fig. 3) demonstrate that this picture may change if the system is biased. In the case of intermediate bias,  $\Delta_B = 50$  meV, the role of real spin and valley isospin are reversed: here, the valley degree of freedom is maximized first. In the case of stronger bias, here for  $\Delta_B = 400$  meV, the properties of the orbital isospin polarization can be altered: we observe states which are antiferromagnetically polarized in the orbital degree of freedom.

A remark about the generality of these statements is in order: the examples we show in Fig. 3 represent cuts through the broadest phases of the phase diagrams we show in Fig. 2 for all the different  $\nu$ . Due to the rich structure apparent from Fig. 2 exhibiting a variety of different phases, many cuts through the phase diagrams are possible which yield octet polarization diagrams different from the ones shown in Fig. 3.

The electronic distribution between the two graphene layers has frequently been discussed in previous works<sup>14,32,33</sup>, in relation with the formation of states exhibiting either interlayer coherence or being fully layer polarized. This is related to the formation of electronic dipoles<sup>14</sup> or the anomalous condensation of excitons<sup>34</sup>. These studies, however, have been carried out within the effective two-band model of BLG<sup>28</sup>. In this approximate description, there is a direct correspondence between the value of the valley index assigned to the electrons and the graphene layer. Therefore, this model automatically predicts a state which is valley-polarized also to be *layer-polarized*. This is not the case in the four-band model. As pointed out in Sec. II B, it is clear from the form of the four-spinor states, Eq. 7, together with the behavior of the coefficients for the respective entries given in Eq. 8 that the one-to-one correspondence between valley index and layer occupation is not exact in the description using all four bands. While for electrons occupying the  $n = 0$  orbital the identification valley  $\leftrightarrow$  layer can still be made, for electrons in the  $n = 1$  orbital also for a well-defined valley index  $+$  or  $-$ , occupation of both layers is enforced as soon as the bias  $\Delta_B$  takes non-zero values. This implies important consequences for the properties of the phases we identified in the phase diagrams of Fig. 2.

Phase \ $\nu$	1	2	3
$\Delta_B \equiv 0$	$\mathbf{S} = \frac{3}{2}\mathbf{e}_z$ $\mathbf{T} = \frac{1}{2}\mathbf{e}_x$ $\mathbf{L} = -\frac{1}{2}\sin 2\theta\mathbf{e}_x + \frac{1}{2}\cos 2\theta\mathbf{e}_z$	$\mathbf{S} = \mathbf{e}_z$ $\mathbf{T} = \mathbf{e}_x$ $\mathbf{L} \equiv 0$	$\mathbf{S} = \frac{1}{2}\mathbf{e}_z$ $\mathbf{T} = \frac{1}{2}\mathbf{e}_x$ $\mathbf{L} = \frac{1}{2}\sin 2\theta\mathbf{e}_x - \frac{1}{2}\cos 2\theta\mathbf{e}_z$
I	$\mathbf{S} = \frac{3}{2}\mathbf{e}_z$ $0 \leq T_z, T_x \leq \frac{1}{2}, T_y \equiv 0$ $0 \leq L_z, L_x \leq \frac{1}{2}, L_y \equiv 0$	$\mathbf{S} = \mathbf{e}_z$ $\mathbf{T} = \sin 2\theta\mathbf{e}_x - \cos 2\theta\mathbf{e}_z$ $\mathbf{L} \equiv 0$	$\mathbf{S} = \frac{1}{2}\mathbf{e}_z$ $0 \leq T_z, T_x \leq \frac{1}{2}, T_y \equiv 0$ $0 \leq L_z, L_x \leq \frac{1}{2}, L_y \equiv 0$
II	$\mathbf{S} = \frac{3}{2}\mathbf{e}_z$ $\mathbf{T} = \frac{1}{2}\sin 2\theta\mathbf{e}_x + \frac{1}{2}\cos 2\theta\mathbf{e}_z$ $\mathbf{L} = \frac{1}{2}\mathbf{e}_z$	$\mathbf{S} = \mathbf{e}_z$ $\mathbf{T} = \mathbf{e}_z$ $\mathbf{L} \equiv 0$	$\mathbf{S} = \frac{1}{2}\mathbf{e}_z$ $\mathbf{T} = -\frac{1}{2}\sin 2\theta\mathbf{e}_x + \frac{1}{2}\cos 2\theta\mathbf{e}_z$ $\mathbf{L} = \frac{1}{2}\mathbf{e}_z$
III	$\mathbf{S} = \frac{3}{2}\mathbf{e}_z$ $\mathbf{T} = \frac{1}{2}\mathbf{e}_z$ $\mathbf{L} = \frac{1}{2}\sin 2\theta\mathbf{e}_x + \frac{1}{2}\cos 2\theta\mathbf{e}_z$	$\mathbf{S} \equiv 0$ $\mathbf{T} = \mathbf{e}_z$ $\mathbf{L} = \mathbf{e}_z$	$\mathbf{S} = \frac{1}{2}\mathbf{e}_z$ $\mathbf{T} = \frac{1}{2}\mathbf{e}_z$ $\mathbf{L} = \frac{1}{2}\sin 2\theta\mathbf{e}_x + \frac{1}{2}\cos 2\theta\mathbf{e}_z$
IV	$\mathbf{S} = \frac{3}{2}\mathbf{e}_z$ $\mathbf{T} = \frac{1}{2}\mathbf{e}_z$ $\mathbf{L} = \frac{1}{2}\mathbf{e}_z$	-	$\mathbf{S} = \frac{1}{2}\mathbf{e}_z$ $\mathbf{T} = \frac{1}{2}\mathbf{e}_z$ $\mathbf{L} = \frac{1}{2}\mathbf{e}_z$
V	$\frac{1}{2} \leq S_z \leq \frac{3}{2}, S_x \equiv S_y \equiv 0$ $\frac{1}{2} \leq T_z \leq \frac{3}{2}, T_x \equiv T_y \equiv 0$ $0 \leq L_z, L_x \leq \frac{1}{2}, L_y \equiv 0$	-	-
VI	$\mathbf{S} = \frac{1}{2}\mathbf{e}_z$ $\mathbf{T} = \frac{3}{2}\mathbf{e}_z$ $\mathbf{L} = \frac{1}{2}\sin 2\theta\mathbf{e}_x + \frac{1}{2}\cos 2\theta\mathbf{e}_z$	-	-
VII	$\mathbf{S} = \frac{1}{2}\mathbf{e}_z$ $\mathbf{T} = \frac{3}{2}\mathbf{e}_z$ $\mathbf{L} = \frac{1}{2}\mathbf{e}_z$	-	-

TABLE X: Spin and isospin properties of the different phases for the bilayer system at positive fillings

In general, valley polarized phases can not be automatically identified with fully layer polarized states. In fact, as evident from the form of the state in Eq. 7, full layer polarization can only be achieved if two conditions are met simultaneously: the electrons must form a state polarized in the valley degree of freedom and at the same time all of them exclusively occupy the  $n = 0$  orbital. We observe phases fulfilling these two requirements in the large bias regime of the two smallest filling factor: in phase (V) at filling factor  $\nu = -3$  and in phase (III) for filling  $\nu = -2$ . The other states at negative filling factors  $\nu = -1$  and  $\nu = 0$ , respectively, tend towards partially polarized states in the limit of large  $\Delta_B$ . Although the overall orbital isospin is partially negatively polarized along the  $z$ -axis, in these cases not only  $n = 0$ , but also  $n = 1$  orbitals are partially occupied. Therefore, the layer occupation does not tend towards exact layer polarization. Nevertheless, in this regime we do find states in which the occupation of one of the two layers largely dominates over the occupation of the other layer. This, however, is not the case for the positive filling factors  $\nu = 1, 2, 3$ . In these cases the states at large bias exhibit overall positive orbital polarization, hence occupation of the  $n = 1$  orbital dominates over occupation of the  $n = 0$  state. As a consequence, no such thing as full layer polarization can be seen. Even in the limit of large bias, the electrons will be distributed between both layers. Furthermore, for the unbiased system at  $\Delta_B \equiv 0$ , we observe the electrons to be equally distributed between both graphene layers for all values of the filling factor  $\nu \in [-3, 3]$ . We illustrate these different types of behavior for the examples  $\nu = -3, \nu = 0, \nu = 1$ , and  $\nu = 3$  in Fig. 4.

### B. Extrapolation to zero magnetic Field

Experiments have studied in detail the limit of vanishing magnetic field. Indeed it has been argued that in the absence of any magnetic field, there is magnetic ordering of the spin and isospin degrees of freedom that spontaneously breaks underlying symmetries<sup>33,35–37</sup> and this may lead to spontaneous QH states<sup>32,38,39</sup>. Furthermore, it has been discussed how these spontaneous QH states might be related to the QH states at nonzero magnetic field<sup>40,41</sup>. Recent experimental investigation draws the following picture: for charge neutral BLG, the existence of a gapped phase at

$\nu$	Phase	GS in the limit $B \rightarrow 0$
-3	$\Delta_B \equiv 0$ (IV)	$ v_1\rangle = \frac{1}{2} [  1, \uparrow, +\rangle +  1, \uparrow, -\rangle +  0, \uparrow, +\rangle +  0, \uparrow, -\rangle ]$ $ v_1\rangle = \frac{1}{\sqrt{2}} [  0, \uparrow, +\rangle +  1, \uparrow, +\rangle ]$
-2	$\Delta_B \equiv 0$ (II)	$ v_1\rangle = \frac{1}{\sqrt{2}} [  1, \uparrow, +\rangle +  1, \uparrow, -\rangle ],  v_2\rangle = \frac{1}{\sqrt{2}} [  0, \uparrow, +\rangle +  0, \uparrow, -\rangle ]$ $ v_1\rangle =  1, \uparrow, +\rangle,  v_2\rangle =  0, \uparrow, +\rangle$
-1	$\Delta_B \equiv 0$ (VI)	$ v_1\rangle = -\frac{1}{\sqrt{2}} [  1, \uparrow, +\rangle +  1, \uparrow, -\rangle ],  v_2\rangle = \frac{1}{\sqrt{2}} [  0, \uparrow, +\rangle +  0, \uparrow, -\rangle ],$ $ v_3\rangle = -\frac{1}{2} [  1, \uparrow, +\rangle -  1, \uparrow, -\rangle +  0, \uparrow, +\rangle -  0, \uparrow, -\rangle ]$ $ v_1\rangle =  1, \uparrow, +\rangle,  v_2\rangle =  0, \uparrow, +\rangle,  v_3\rangle = \frac{1}{\sqrt{2}} [  1, \downarrow, +\rangle +  0, \downarrow, +\rangle ]$
0	$\Delta_B \equiv 0$ (III)	$ v_1\rangle =  1, \uparrow, +\rangle,  v_2\rangle =  1, \uparrow, -\rangle,  v_3\rangle =  0, \uparrow, +\rangle,  v_4\rangle =  0, \uparrow, -\rangle$ $ v_1\rangle =  1, \uparrow, +\rangle,  v_2\rangle =  1, \downarrow, +\rangle,  v_3\rangle =  0, \uparrow, +\rangle,  v_4\rangle =  0, \downarrow, +\rangle$
1	$\Delta_B \equiv 0$ (VI)	$ v_1\rangle =  1, \uparrow, +\rangle,  v_2\rangle =  1, \uparrow, -\rangle,  v_3\rangle =  0, \uparrow, +\rangle,  v_4\rangle =  0, \uparrow, -\rangle,$ $ v_5\rangle = \frac{1}{2} [  1, \downarrow, +\rangle +  1, \downarrow, -\rangle -  0, \downarrow, +\rangle -  0, \downarrow, -\rangle ]$ $ v_1\rangle =  1, \uparrow, +\rangle,  v_2\rangle =  1, \downarrow, +\rangle,  v_3\rangle =  0, \uparrow, +\rangle,  v_4\rangle =  0, \downarrow, +\rangle,  v_5\rangle = \frac{1}{\sqrt{2}} [  1, \uparrow, -\rangle +  0, \uparrow, -\rangle ]$
2	$\Delta_B \equiv 0$ (II)	$ v_1\rangle =  1, \uparrow, +\rangle,  v_2\rangle =  1, \uparrow, -\rangle,  v_3\rangle =  0, \uparrow, +\rangle,  v_4\rangle =  0, \uparrow, -\rangle,$ $ v_5\rangle = \frac{1}{\sqrt{2}} [  1, \downarrow, +\rangle +  1, \downarrow, -\rangle ],  v_6\rangle = \frac{1}{\sqrt{2}} [  0, \downarrow, +\rangle +  0, \downarrow, -\rangle ]$ $ v_1\rangle =  1, \uparrow, +\rangle,  v_2\rangle =  1, \uparrow, -\rangle,  v_3\rangle =  0, \uparrow, +\rangle,  v_4\rangle =  0, \uparrow, -\rangle,  v_5\rangle =  1, \downarrow, +\rangle,  v_6\rangle =  0, \downarrow, +\rangle$
3	$\Delta_B \equiv 0$ (III)	$ v_1\rangle =  1, \uparrow, +\rangle,  v_2\rangle =  1, \uparrow, -\rangle,  v_3\rangle =  0, \uparrow, +\rangle,  v_4\rangle =  0, \uparrow, -\rangle,  v_5\rangle = \frac{1}{2} [  1, \downarrow, +\rangle +  1, \downarrow, -\rangle +  0, \downarrow, +\rangle +  0, \downarrow, -\rangle ],$ $ v_6\rangle = \frac{1}{2} [  1, \downarrow, +\rangle +  1, \downarrow, -\rangle -  0, \downarrow, +\rangle -  0, \downarrow, -\rangle ],  v_7\rangle = \frac{1}{2} [  1, \downarrow, +\rangle -  1, \downarrow, -\rangle +  0, \downarrow, +\rangle -  0, \downarrow, -\rangle ]$ $ v_1\rangle =  1, \uparrow, +\rangle,  v_2\rangle =  1, \uparrow, -\rangle,  v_3\rangle =  0, \uparrow, +\rangle,  v_4\rangle =  0, \uparrow, -\rangle,$ $ v_5\rangle =  1, \downarrow, +\rangle,  v_6\rangle =  0, \downarrow, +\rangle,  v_7\rangle = \frac{1}{\sqrt{2}} [  1, \downarrow, -\rangle +  0, \downarrow, -\rangle ]$

TABLE XI: States in the limit  $B \rightarrow 0$ 

zero magnetic field in sufficiently clean samples at sufficiently low temperatures is generally established<sup>4,42</sup>. This phase evolves continuously in the gapped  $\nu = 0$  QH state as the magnetic field increases<sup>2,5,43</sup>. For filling factor  $\nu = 2$ , the observations of Ref. 7 suggest that the behavior with  $B \rightarrow 0$  depends on the bias potential applied: while for small  $\Delta_B$  the system extrapolates to vanishing gap, for sufficiently large bias, when the system presumably has entered a phase different from the low bias phase, the gap remains finite as  $B$  goes to zero. Reference 10 reports for  $\nu = 1$  a vanishing gap with vanishing magnetic field independently of the bias potential, e.g., for the two different phases observed in this study. We now analyze the limit  $B \rightarrow 0$  in our approach. We summarize for each filling factor the properties of the unbiased case  $\Delta_B \equiv 0$ , as well as the phases that extend to the low magnetic field regime of the phase diagrams in Fig. 2. For the odd filling factors these phases go along with canting of the orbital degree of freedom (phase (IV) at  $\nu = -3$ , phase (VI) at  $\nu = -1$ , phase (VI) at  $\nu = 1$ ). To understand the behavior at low magnetic field, we show the evolution as a function of  $B$  of the different canting angles in these respective phases as well as the orbital canting angles of the zero bias phases in Fig. 5. The states which follow from the naive extrapolation  $B \rightarrow 0$  are summarized in Table XI. While for even filling factors  $\nu = -2, 0, 2$  the GS configurations decompose into simple product states in the orbital degree of freedom, at odd fillings  $\nu = -3, -1, +1, +3$  we find states with non-trivial orbital coherence in the limit  $B \rightarrow 0$ . These orbitally coherent states explicitly rely on the quantization of the LL modes by the external magnetic field and thus do not have an obvious counterpart in the zero-field case. This means that the states at odd filling factors behave differently from the even filling factor states when the field is decreased to zero. While at even fillings the GS might be connected smoothly to gapped spontaneous QH states at  $B = 0$ , such extrapolation is not obvious for odd filling factors. Here, the zero magnetic field GS might be gapless. Indications for such behavior have been seen experimentally, e.g., in Refs. 2,5,43, and 10. We note, however, that the description of BLG in our model is valid really only in the limit of high magnetic fields since LL mixing will be important at low fields. The states we extract for  $B \rightarrow 0$  in Table XI can serve only as hints to connect the high magnetic field region and the case  $B = 0$  where spontaneous QH states have been predicted. We can not exclude the existence of additional phases in the regime of small but nonzero magnetic field, as conjectured, e.g., in Refs. 2 or 40.

## VI. RELATION TO EXPERIMENT AND TO THEORETICAL STUDIES

The effect of external magnetic and electric fields on graphene mono- and multilayers has been under intense experimental investigation<sup>2–11</sup>. We first compare our work with experimental findings, before discussing similarities and differences with theoretical approaches<sup>13–15,19</sup>. The fact that external fields influence the ordering of spin, valley, and orbital degrees of freedom, and that transitions between states of different spin and isospin order can be induced by tuning externally applied fields has been realized several years ago<sup>2,3</sup>. Recently, there has been tremendous improvement in the quality of the samples, and data became available in a much wider parameter range. This has lead to detailed insights about the nature of the different phases at different filling factors. By carefully monitoring sudden changes in the conduction properties, one infers the number of phase transitions upon varying the bias potential at fixed magnetic field  $B$ . At  $\nu = \pm 3$ , a single phase transition has been seen<sup>2,6,9</sup> at zero bias  $\Delta_B \equiv 0$ . For  $\nu = \pm 2$ , Refs. 2,7–9,11 report transitions at nonzero bias while there is no sign of phase transition at zero bias. Both types of transitions, at  $\Delta_B \equiv 0$  as well as at  $|\Delta_B| \neq 0$ , have been observed<sup>2,9–11</sup> at  $\nu = \pm 1$ . The properties at charge neutrality  $\nu = 0$  have been investigated in Refs. 2–6,8,11. While early investigations reported one transition at nonzero bias<sup>2,3</sup>, more recent studies report signatures of transitions at two different values of the bias potential implying at least three different phases. Common belief is that for large bias potential the system will be in a spin and isospin configuration that maximizes layer polarization. Accordingly, in the opposite limit of very small or vanishing bias, the spin and isospin ordering is assumed to be different from maximally possible layer polarization.

We compare these experimental observations to the predictions of our calculations. In parameter ranges comparable to those of the respective experiments, we examine the different phases and the number of phase transitions at fixed magnetic and increasing bias:

\* For filling factor  $\nu = -3$ , we obtain the following picture: for  $B < 11$  T we see the sequence of transitions (I)  $\rightarrow$  (IV)  $\rightarrow$  (V), whereas for higher magnetic fields  $B > 11$  T the series of transitions (II)  $\rightarrow$  (III)  $\rightarrow$  (IV)  $\rightarrow$  (V) is observed.

Maher et al. 9 as well as Hunt et al. 11 have studied the BLG system at  $\nu = \pm 3$  h in the range of the bias  $|\Delta_B| \approx 0 - 34$  meV for magnetic fields  $B = 9$  T and  $B = 31$  T, respectively. We may attribute the single transition close to zero bias observed in both references to the transitions (I)  $\rightarrow$  (IV) at lower magnetic field or (II)  $\rightarrow$  (III) at higher magnetic field value, respectively. The values of the bias potential at which these transitions occur in our model are both small compared to the energy scales of the other phases of the phase diagram:  $\Delta_B \approx 0.185$  meV and  $\Delta_B \approx 2.5$  meV, respectively. The fact that no second phase transition is observed by Hunt et al. 11 may imply that phase (IV) has not yet been reached at these values of the bias. If the zero-bias phases we find in the HF treatment are destroyed by fluctuations beyond HF then this may explain a zero-bias transition between oppositely polarized states.

\* For  $\nu = \pm 2$  we see for all values of the magnetic field the sequence of transitions (I)  $\rightarrow$  (II)  $\rightarrow$  (III) as a function of increasing bias. The second transition (II)  $\rightarrow$  (III), however, occurs at much higher values of the bias potential than those shown in experimental data:  $\Delta_B \gtrsim 300$  meV in Fig. 2. Our predictions are consistent with the observations at  $\nu = \pm 2$  of Velasco et al. 7, Maher et al. 9, Hunt et al. 11, Lee et al. 8 identifying one phase transition at nonzero bias  $\Delta_B > 0$ . So the low-bias phase has valley coherence and this coherence is destroyed beyond a critical bias. The slope of the I/II transition line in Velasco et al. is  $0.72 \text{ mV nm}^{-1} \text{ T}^{-1}$  while the HF value is  $0.55 \text{ mV nm}^{-1} \text{ T}^{-1}$ .

\* At filling  $\nu = -1$  for magnetic fields  $B < 11.3$  T, we go through the sequence (I)  $\rightarrow$  (III)  $\rightarrow$  (VI)  $\rightarrow$  (VII), in the opposite case  $B > 11.3$  T we find (II)  $\rightarrow$  (IV)  $\rightarrow$  (V)  $\rightarrow$  (VI)  $\rightarrow$  (VII) when increasing  $\Delta_B$ . In the case  $\nu = +1$ , at small magnetic field  $B < 11.3$  T, the sequence is (I)  $\rightarrow$  (III)  $\rightarrow$  (VI) / (VII), whereas for larger field  $B > 11.3$  T it is (II)  $\rightarrow$  (IV)  $\rightarrow$  (V)  $\rightarrow$  (VI).

This may be compared to the experimental results of Shi et al. 10, Hunt et al. 11, and Maher et al. 9, where the states  $\nu = \pm 1$  are probed for  $B = 28$  T in the range  $|\Delta_B| \approx 0 - 17$  meV, and in the range  $|\Delta_B| \approx 0 - 34$  meV at magnetic fields  $B = 31$  T and  $B = 9$  T, respectively. The observed transition near zero bias can be attributed to the phase transitions (I)  $\rightarrow$  (III) or (II)  $\rightarrow$  (IV), respectively, which occur in our model at relatively small values of  $\Delta_B$  compared to the range of the broadest phases of the phase diagram and to the overall range of the bias. The phase II has valley coherence as proposed in Shi et al. A second transition observed in experiment at nonzero value of the bias might be identified with the transitions (III)  $\rightarrow$  (VI) or (IV)  $\rightarrow$  (V)/(VI) at  $\nu = -1$  and (III)  $\rightarrow$  (VI) / (VII) or (IV)  $\rightarrow$  (V)/(VII) at  $\nu = 1$ , respectively. In fact Maher et al. have proposed that the finite bias transition they see at  $\nu = +1$  is the IV/VII transition.

\* In the  $\nu = 0$  case, for any value of the magnetic field, we observe two successive phase transitions (I)  $\rightarrow$  (II)  $\rightarrow$  (III) upon increasing bias potential. The phase II is a spin-valley coherent phase flanked by simpler incoherent phases I, III. This is consistent with recent experimental studies of the  $\nu = 0$  state by Lee et al. 8 and Hunt et al. 11, where two transitions at two distinct nonzero values of the bias potential have been observed. The  $\nu = 0$  phase diagram shown in Ref. 11 Fig. 2D also agrees well with the corresponding phase diagram predicted by our calculations. Furthermore, Maher et al. 6 have also observed a critical bias increasing as a function of the magnetic field.

From this discussion we see that our calculation reproduces several features observed experimentally in BLG at different filling factors. Notably, for every  $\nu$ , we are able to identify phase transitions detected in experiment with transitions predicted by our model. The range of the bias achieved in the various different experimental studies only covers part of the phase diagrams presented in Fig. 2. In particular the phase of maximal orbital polarization, corresponding the phase with the highest number in each case, presumably has not been reached in experiments for the filling factors  $\nu = -3, \nu = -2, \nu = -1$ , and  $\nu = 2$ . As a consequence, according to the properties of the four-band model as discussed in Sec. V, maximally possible layer polarization has not been achieved experimentally. Furthermore, from the phase diagrams of Fig. 2, we conjecture that for example at fillings  $\nu = -3$  or  $\nu = 1$  a richer picture of different phases and phase transitions may emerge for an extended range of  $B$  and  $\Delta_B$ .

It should be noted, however, that the various experiments often differ in the way the sample is prepared, e.g., Refs. 2,5,7,10 investigate the properties of suspended BLG, Ref. 8 uses double BLG heterostructures separated by a hexagonal boron nitride dielectric while in Refs. 6,9,11 the BLG samples are encapsulated by hexagonal boron nitrate. We have not tried to take into account the additional effects due to these different substrates, gatings, dielectrics, or encapsulations. These differences may change the physics of the phase competition.

Let us now compare our results to previous theoretical investigations. Ref. 19 presents a detailed HF study of BLG zero energy octet with an effective two-band model. They obtained the phase diagram of their model for all different filling factors  $\nu \in [-3, 3]$  for  $B = 10$  T as a function of the bias. The vast majority of states they deduce from their model is orbitally incoherent. Phases exhibiting orbital coherence emerge only at very large values of the bias. These authors do not take into account the presence of the Dirac sea. It has become clear, however, that these electrons of the Dirac sea do play a non-silent role: As we discuss in Sec. IIB, Shizuya shows in Ref. 15 in a four-band model the importance of this effect. The GS configurations identified in this treatment e.g. at zero bias can be coherent superpositions of the  $n = 0$  and  $n = 1$  states. Moreover, in this analysis, the  $n = 1$  state lies lower in energy than the  $n = 0$  orbital while in Ref. 19 generally the  $n = 0$  state is populated first. These results, however, were obtained from a somewhat simplified model with respect to Lambert and Côté in Ref. 19.

Our treatment contains the ingredient of a realistic band structure, i.e., four bands with all the  $\gamma_i$  couplings and we have included the Dirac sea exchange.

## VII. CONCLUSION

We have derived the phase diagram of the Bernal-stacked bilayer graphene as a function of the applied magnetic field and potential bias between the layers. We have focused on the octet of levels near neutrality for which the filling factor is in the range  $[-3, +3]$ . We have used a HF method which is known to capture the main features of quantum Hall ferromagnetism. Our tight-binding model includes hoppings  $\gamma_0, \gamma_1, \gamma_3, \gamma_4$  that breaks weakly particle-hole symmetry and we have retained the four bands. In the HF calculation we have included the exchange within the occupied Dirac sea which restores the particle-hole symmetry in the absence of  $\gamma_4$ . The splitting between  $n = 0$  and  $n = 1$  orbitals is thus governed by the competition between band structure effects and Lamb-shift-like exchange interactions. The spin and isospin configuration hence is governed by a careful balance between all these different symmetry breaking terms. This is illustrated in Fig. 6, where we show the evolution of the energy splittings in spin space, valley isospin space, and orbital isospin space,  $\Delta_Z, \Delta_{B,eff}$ , and  $\Delta_{01}$ , as well as the matrix elements of the Coulomb interaction as computed in Sec. IIB as functions of the external magnetic and electric fields for different parameters. In the regime of small bias and large magnetic field,  $\Delta_{01}$  plays a pivotal role before being washed out at sufficiently strong bias by  $\Delta_{B,eff}$  acting as a "Zeeman-like" splitting in valley space.

For even filling factors  $\nu = 0, \pm 2$  our results are the same as the HF treatment of Lambert and Côté<sup>19</sup>. However for odd fillings  $\nu = \pm 1, \pm 3$  we find phases with non-trivial orbital coherence: see Fig. 2. These phases are thus of fundamentally different nature than those predicted in Ref. 19. As these orbital coherent phases appear at experimentally accessible values of the bias potential, it is plausible that they are among the phases actually observed in experiment. For fillings  $\nu = -3, -1$  they extend to all values of the magnetic field but require a specific range of bias. For  $\nu = +3, +1$  the orbital phases are restricted to the small-field regime which may be out of range of our approach due to Landau level mixing.

For odd filling factors we observe at small bias a transition from an orbital coherent phase to orbitally incoherent phases as a function of the magnetic field strength: the vector of orbital isospin rotates from a canted position at small magnetic field to a partially polarized configuration above a critical field strength  $B_{crit}$ . Such transitions with  $B$  have not been reported previously in the literature as e.g. Ref. 19 restricts its investigations of the GS phases to the phase diagram at a single fixed value of the magnetic field. We conclude that varying the magnetic field can trigger the emergence of phase transitions for all odd  $\nu$ . We thus conjecture the existence of more phases and even richer phase diagrams when the BLG is studied over a sufficiently large range of  $B$  values.

## Acknowledgments

We acknowledge discussions with A. H. MacDonald, Feng Cheng Wu, and René Côté. AK would like to thank R. A. Römer for discussions about numerical HF calculations and for pointing out References 30 and 31. AK gratefully acknowledges support by the German Academic Scholarship Foundation and by the German Academic Exchange Service.

- 
- <sup>1</sup> A. Knothe and T. Jolicoeur, Phys. Rev. B **92**, 165110 (2015).
  - <sup>2</sup> R. T. Weitz, M. T. Allen, B. E. Feldman, J. Martin, and A. Yacoby, Science **330**, 812 (2010), ISSN 0036-8075, 1095-9203.
  - <sup>3</sup> S. Kim, K. Lee, and E. Tutuc, Phys. Rev. Lett. **107**, 016803 (2011).
  - <sup>4</sup> W. Bao, J. Velasco, F. Zhang, L. Jing, B. Standley, D. Smirnov, M. Bockrath, A. H. MacDonald, and C. N. Lau, PNAS **109**, 10802 (2012), ISSN 0027-8424, 1091-6490.
  - <sup>5</sup> J. V. Jr, L. Jing, W. Bao, Y. Lee, P. Kratz, V. Aji, M. Bockrath, C. N. Lau, C. Varma, R. Stillwell, et al., Nat Nano **7**, 156 (2012), ISSN 1748-3387.
  - <sup>6</sup> P. Maher, C. R. Dean, A. F. Young, T. Taniguchi, K. Watanabe, K. L. Shepard, J. Hone, and P. Kim, Nat Phys **9**, 154 (2013), ISSN 1745-2473.
  - <sup>7</sup> J. Velasco Jr, Y. Lee, F. Zhang, K. Myhro, D. Tran, M. Deo, D. Smirnov, A. H. MacDonald, and C. N. Lau, Nat Commun **5**, 4550 (2014).
  - <sup>8</sup> K. Lee, B. Fallahazad, J. Xue, D. C. Dillen, K. Kim, T. Taniguchi, K. Watanabe, and E. Tutuc, Science **345**, 58 (2014), ISSN 0036-8075, 1095-9203.
  - <sup>9</sup> P. Maher, L. Wang, Y. Gao, C. Forsythe, T. Taniguchi, K. Watanabe, D. Abanin, Z. Papić, P. Cadden-Zimansky, J. Hone, et al., Science **345**, 61 (2014), ISSN 0036-8075, 1095-9203.
  - <sup>10</sup> Y. Shi, Y. Lee, S. Che, Z. Pi, T. Espiritu, P. Stepanov, D. Smirnov, C. N. Lau, and F. Zhang, Phys. Rev. Lett. **116**, 056601 (2016).
  - <sup>11</sup> B. M. Hunt, J. I. A. Li, A. A. Zibrov, L. Wang, T. Taniguchi, K. Watanabe, J. Hone, C. R. Dean, M. Zaletel, R. C. Ashoori, et al., arXiv:1607.06461 [cond-mat] (2016), 1607.06461.
  - <sup>12</sup> Y. Barlas, R. Côté, K. Nomura, and A. H. MacDonald, Phys. Rev. Lett. **101**, 097601 (2008).
  - <sup>13</sup> E. V. Castro, K. S. Novoselov, S. V. Morozov, N. M. R. Peres, J. M. B. L. dos Santos, J. Nilsson, F. Guinea, A. K. Geim, and A. H. C. Neto, J. Phys.: Condens. Matter **22**, 175503 (2010), ISSN 0953-8984.
  - <sup>14</sup> R. Côté, J. Lambert, Y. Barlas, and A. H. MacDonald, Phys. Rev. B **82**, 035445 (2010).
  - <sup>15</sup> K. Shizuya, Phys. Rev. B **86**, 045431 (2012).
  - <sup>16</sup> E. V. Gorbar, V. P. Gusynin, J. Jia, and V. A. Miransky, Phys. Rev. B **84**, 235449 (2011).
  - <sup>17</sup> B. Roy, Phys. Rev. B **88**, 075415 (2013).
  - <sup>18</sup> B. Roy, Phys. Rev. B **89**, 201401 (2014).
  - <sup>19</sup> J. Lambert and R. Côté, Phys. Rev. B **87**, 115415 (2013).
  - <sup>20</sup> J. W. McClure, Phys. Rev. **108**, 612 (1957).
  - <sup>21</sup> J. C. Slonczewski and P. R. Weiss, Phys. Rev. **109**, 272 (1958).
  - <sup>22</sup> E. McCann and M. Koshino, Rep. Prog. Phys. **76**, 056503 (2013), ISSN 0034-4885.
  - <sup>23</sup> A. B. Kuzmenko, I. Crassee, D. van der Marel, P. Blake, and K. S. Novoselov, Phys. Rev. B **80**, 165406 (2009).
  - <sup>24</sup> M. Yankowitz, J. I.-J. Wang, S. Li, A. G. Birdwell, Y.-A. Chen, K. Watanabe, T. Taniguchi, S. Y. Quek, P. Jarillo-Herrero, and B. J. LeRoy, APL MATERIALS **2**, 092503 (2014), ISSN 2166-532X, 1406.0898.
  - <sup>25</sup> M. Mucha-Kruczyński, O. Tsyplatyev, A. Grishin, E. McCann, V. I. Fal'ko, A. Bostwick, and E. Rotenberg, Phys. Rev. B **77**, 195403 (2008).
  - <sup>26</sup> M. Mucha-Kruczyński, D. S. L. Abergel, E. McCann, and V. I. Fal'ko, J. Phys.: Condens. Matter **21**, 344206 (2009), ISSN 0953-8984.
  - <sup>27</sup> M. Mucha-Kruczyński, *Theory of Bilayer Graphene Spectroscopy*, Springer Theses (Springer Berlin Heidelberg, Berlin, Heidelberg, 2013), ISBN 978-3-642-30935-9 978-3-642-30936-6.
  - <sup>28</sup> E. McCann and V. I. Fal'ko, Phys. Rev. Lett. **96**, 086805 (2006).
  - <sup>29</sup> C. C. J. Roothaan, Rev. Mod. Phys. **23**, 69 (1951).
  - <sup>30</sup> C. Sohrmann and R. A. Römer, New J. Phys. **9**, 97 (2007), ISSN 1367-2630.
  - <sup>31</sup> R. A. Römer and C. Sohrmann, phys. stat. sol. (b) **245**, 336 (2008), ISSN 1521-3951.
  - <sup>32</sup> F. Zhang and A. H. MacDonald, Phys. Rev. Lett. **108**, 186804 (2012).
  - <sup>33</sup> H. Min, G. Borghi, M. Polini, and A. H. MacDonald, Phys. Rev. B **77**, 041407 (2008).
  - <sup>34</sup> Y. Barlas, R. Côté, J. Lambert, and A. H. MacDonald, Phys. Rev. Lett. **104**, 096802 (2010).
  - <sup>35</sup> F. Zhang, H. Min, M. Polini, and A. H. MacDonald, Phys. Rev. B **81**, 041402 (2010).
  - <sup>36</sup> R. Nandkishore and L. Levitov, Phys. Rev. B **82**, 115124 (2010).
  - <sup>37</sup> J. Jung, F. Zhang, and A. H. MacDonald, Phys. Rev. B **83**, 115408 (2011).
  - <sup>38</sup> F. Zhang, J. Jung, G. A. Fiete, Q. Niu, and A. H. MacDonald, Phys. Rev. Lett. **106**, 156801 (2011).
  - <sup>39</sup> F. Zhang, H. Min, and A. H. MacDonald, Phys. Rev. B **86**, 155128 (2012).
  - <sup>40</sup> R. Nandkishore and L. Levitov, arXiv:1002.1966 [cond-mat] (2010), 1002.1966.

<sup>41</sup> M. Kharitonov, Phys. Rev. Lett. **109**, 046803 (2012).

<sup>42</sup> F. Freitag, J. Trbovic, M. Weiss, and C. Schönenberger, Phys. Rev. Lett. **108**, 076602 (2012).

<sup>43</sup> A. Veligura, H. J. van Elferen, N. Tombros, J. C. Maan, U. Zeitler, and B. J. van Wees, Phys. Rev. B **85**, 155412 (2012).

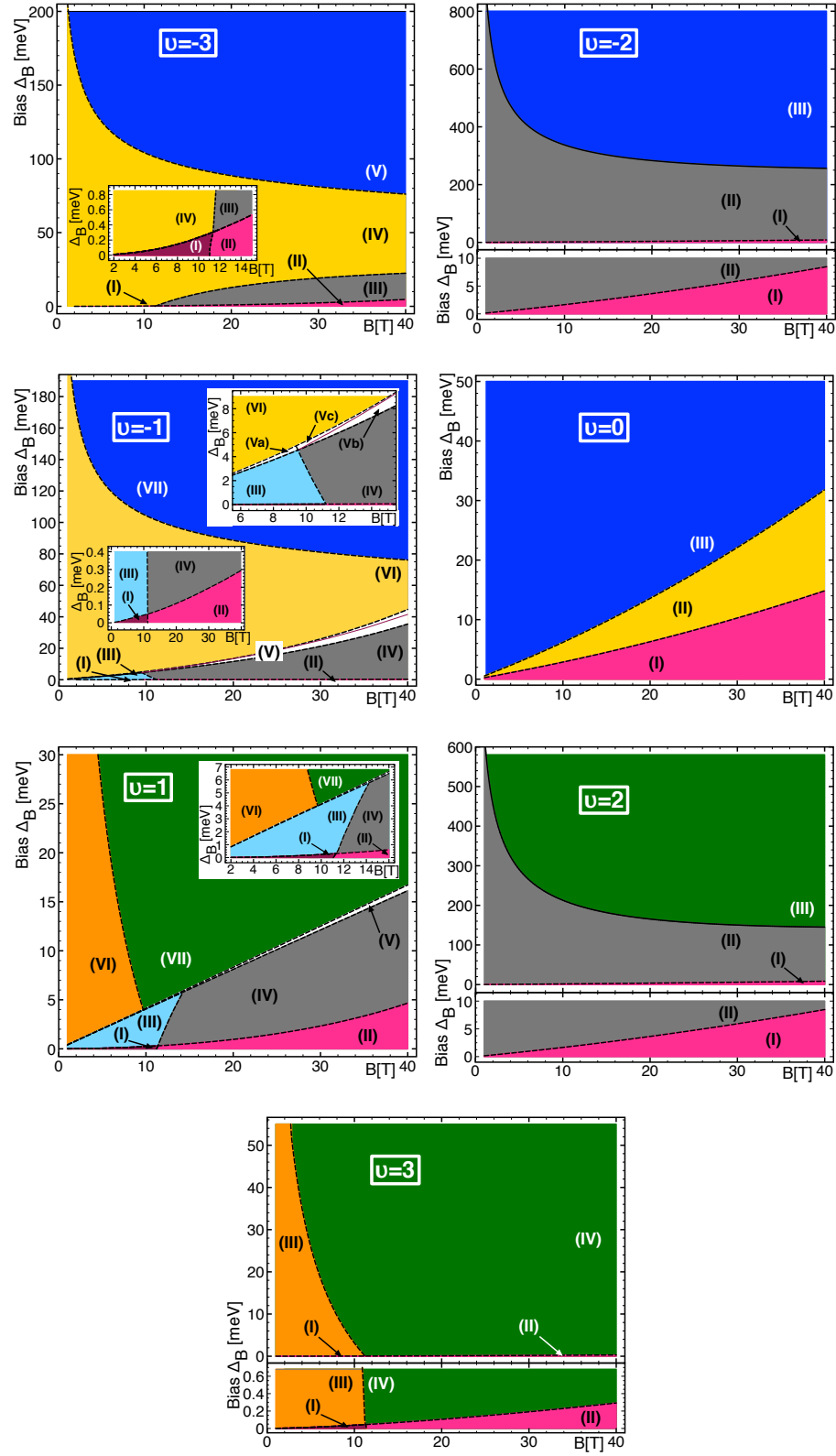


FIG. 2: Phase diagrams obtained for BLG at the different filling factors  $\nu \in [-3, 3]$ . The GS behavior of the Hamiltonian  $H_{HF}$  of Eq. 19 is studied with the HF methods described in Sec. II C. We employ the following color code for the phases: bordeaux/magenta:  $\mathbf{S} \propto \mathbf{e}_z$  and  $\mathbf{T}$  in a canted state  $\rightarrow$  valley coherence; yellow/orange:  $\mathbf{S} \propto \mathbf{e}_z$  and  $\mathbf{L}$  in a canted state  $\rightarrow$  orbital coherence; gray/blue/green:  $\mathbf{S}, \mathbf{T} \propto \mathbf{e}_z$  for  $\mathbf{L} \equiv 0$  or  $\mathbf{L} \propto \pm \mathbf{e}_z \rightarrow$  partial polarization.



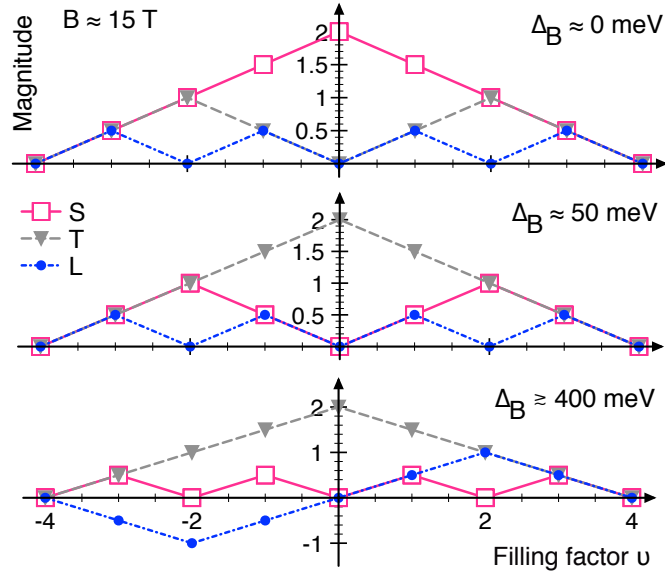


FIG. 3: Octet polarization properties: At magnetic field  $B = 15$  T and for different values of the bias potential  $\Delta_B$ , we plot the magnitude of the spin vector (pink, solid line, empty squares), the valley isospin vector (gray, dashed line, filled triangles) and the orbital isospin vector (blue, dashed-dotted line, filled circles) as a function of the filling factor  $\nu$ . The values of  $B$  and  $\Delta_B$  are chosen as representative examples, similar behavior occurs over a broad parameter range in throughout the phase diagrams. The *magnitude* of an isospin vector is to be understood as  $\text{magnitude}[\mathbf{e}_z] = \text{magnitude}[\mathbf{e}_x] = 1$ .

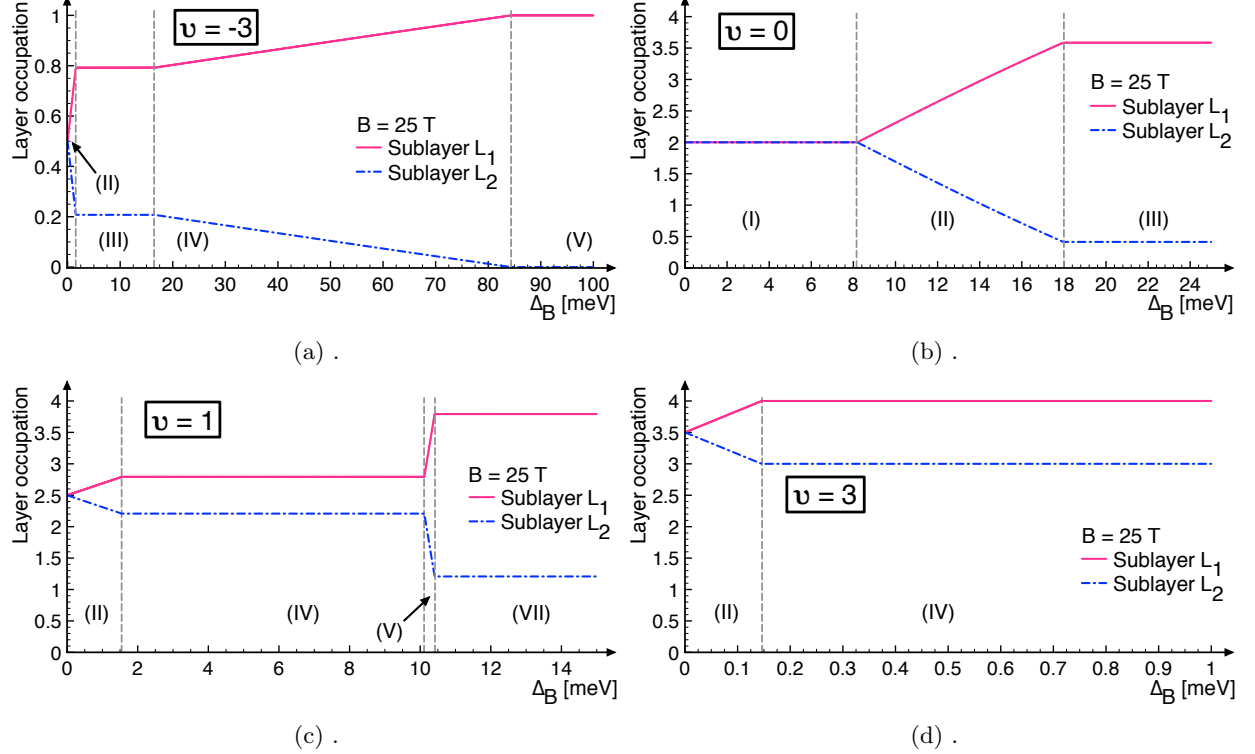


FIG. 4: Electronic distribution between the two sublayers, labeled as layer 1 and layer 2, in different phases at filling factors  $\nu = -3, \nu = 0, \nu = 1$ , and  $\nu = 3$ .

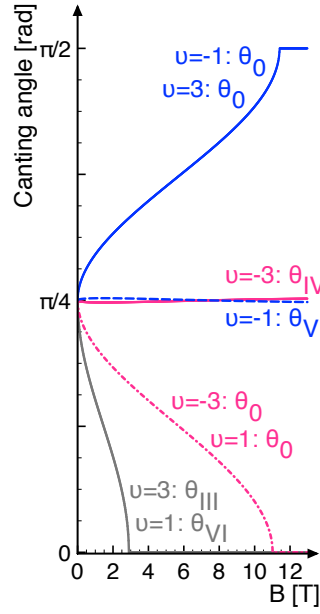


FIG. 5: Canting angles in orbital space at different filling factors at low magnetic field: Blue curves for  $\nu = -1$  or  $\nu = 3$ : Unbiased case  $\theta_0$  according to Eqs. 31, 54 (solid line) and phase (VI)  $\theta_{VI}$  according to Eq. 34 (dashed line). Pink curves at  $\nu = -3$  or  $\nu = 1$ : Phase (IV)  $\theta_{IV}$  according to Eq. 24 (solid line) and unbiased case  $\theta_0$  according to Eqs. 22, 42 (dashed line). Gray curve at  $\nu = 3$  or  $\nu = 1$ : Phase (III)  $\theta_{III}$  according to Eq. 56 and Phase (VI)  $\theta_{VI}$  according to Eq. 45. For the corresponding angles at filling factors  $\nu = 2$  and  $\nu = -2$  we find  $\theta_0 \equiv \frac{\pi}{4}$  for all  $B$ .

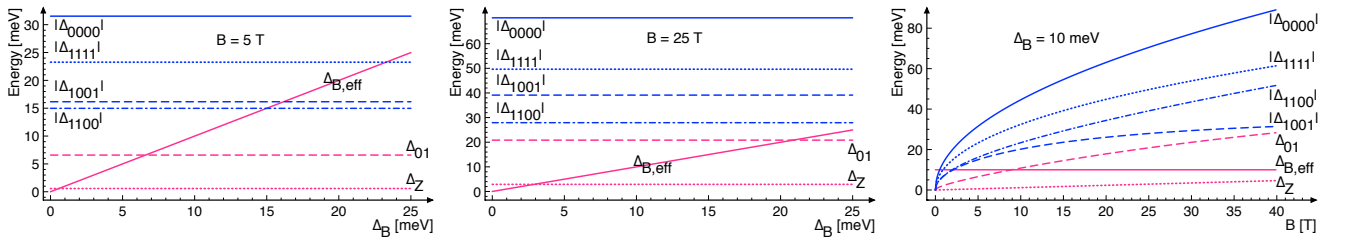


FIG. 6: Dependence on the magnetic field and on the bias potential of the energy splittings in valley space, orbital space, and spin space,  $\Delta_{B,eff}$ ,  $\Delta_{01}$ , and  $\Delta_Z$ , respectively, as well of the valley conserving exchange matrix elements of the Coulomb interaction,  $\Delta_{1111}$ ,  $\Delta_{0000}$ ,  $\Delta_{1001}$ , and  $\Delta_{1100}$ , as computed from Eq. 16. The curves for the valley breaking matrix elements,  $X_{1111}$ ,  $X_{0000}$ ,  $X_{1001}$ , and  $X_{1100}$  are slightly offset with respect to the valley conserving terms but comparable in their overall behavior and are therefore not shown for the sake of visibility.